THE PLANT CELL

The Plant Cell, 2025, **37**, koaf242

https://doi.org/10.1093/plcell/koaf242
Advance access publication 15 October 2025
Research Article

The *CYP71A*, *NIT*, *AMI*, and *IAMH* gene families are dispensable for indole-3-acetaldoxime-mediated auxin biosynthesis in *Arabidopsis*

Mario Fenech,[1] Javier Brumos,[1,†] Aleš Pěnčík,[2] Brianne Edwards,[1] Sara Belcapo,[3] Jennifer DeLacey,[1] Arjun Patel,[1] Martin Kater,[3] Xu Li,[1] Karin Ljung,[4] Ondrej Novak,[2] José M. Alonso,[1,*] Anna N. Stepanova[1,*]

[1]Department of Plant and Microbial Biology, College of Agriculture and Life Sciences, North Carolina State University, Raleigh, NC 27695-7614, USA
[2]Laboratory of Growth Regulators, Institute of Experimental Botany, the Czech Academy of Sciences & Faculty of Science, Palacký University, Olomouc, Czech Republic
[3]Department of BioScience, Università Degli Studi di Milano, Milan, Italy
[4]Department of Forest Genetics and Plant Physiology, Umeå Plant Science Centre (UPSC), Swedish University of Agricultural Sciences, Umeå, Sweden
*Author for correspondence: jmalonso@ncsu.edu (J.M.A.), atstepan@ncsu.edu (A.N.S.)
[†]Present address: Institute for Plant Molecular and Cell Biology (IBMCP), CSIC-Universitat Politècnica de Valencia, Valencia, Spain
The authors responsible for distribution of materials integral to the findings presented in this article in accordance with the policy described in the Instructions for Authors (https://academic.oup.com/plcell/pages/General-Instructions) are: Anna N. Stepanova (atstepan@ncsu.edu) and Jose M. Alonso (jmalonso@ncsu.edu).

Abstract

The auxin indole-3-acetic acid (IAA) governs plant development and environmental responses. Although the indole-3-pyruvic acid (IPyA) pathway is the predominant route for IAA biosynthesis, other pathways have been proposed, such as the indole-3-acetaldoxime (IAOx) pathway. The IAOx pathway has garnered attention due to its supposed activation in auxin-overproducing mutants (e.g. *sur1*, *sur2*, *ugt74b1*) and the auxin-like responses triggered by exogenous application of its proposed intermediates IAOx, indole-3-acetonitrile (IAN), and indole-3-acetamide (IAM). However, despite the supporting evidence for individual steps of the IAOx pathway, its overall physiological relevance remains inconclusive. Here, using a comprehensive genetic approach combined with metabolic and phenotypic profiling, we demonstrate that mutating gene families proposed to function in the IAOx pathway in *Arabidopsis* (*Arabidopsis thaliana*) does not result in prominent auxin-deficient phenotypes, nor are these genes required for the high auxin production in the *sur2* mutant. Our findings also challenge the previously postulated linear IAOx pathway. Exogenously provided IAOx, IAN, and IAM can be converted to IAA in vivo, but they do not act as precursors for each other. Finally, our findings question the physiological relevance of IAM and IAN as IAA precursors in plants and suggest the existence of a yet-uncharacterized route for IAA production in the *sur2* mutant, likely involving IAOx as an intermediate. The identification of the metabolic steps and the corresponding genes in this pathway may uncover another IAA biosynthesis route in plants.

Introduction

The plant hormone auxin plays a central regulatory role in almost every aspect of the plant life cycle, from activating developmental programs to triggering responses to environmental cues (Zhao 2018). The best-characterized auxin, indole-3-acetic acid (IAA), is known to act in a concentration-dependent manner, and thus, its abundance is spatiotemporally regulated through finely controlled and interconnected biosynthetic, transport, and degradation processes (Petricka et al. 2012; Brumos et al. 2018; Hayashi et al. 2021; Zhang et al. 2023). Different genetic, biochemical, metabolic, and phenotypic approaches have been used to identify and characterize the key elements in these processes (Vorwerk et al. 2001; Pollmann et al. 2002, 2006; Müller et al. 2015). In the case of auxin biosynthesis, 2 general routes of IAA production have been proposed based on whether or not they use the amino acid tryptophan (TRP) as a precursor (Fig. 1). The tentative TRP-independent pathway was originally proposed based on radiolabeled indole feeding experiments in maize (*Zea mays*) and *Arabidopsis* (*Arabidopsis thaliana*) TRP biosynthetic mutants (Wright et al. 1991; Normanly et al. 1993; Ostin et al. 1999; Ouyang et al. 2000). These experiments suggested that IAA could be produced not from TRP but from indole derived from upstream TRP precursors. Despite considerable efforts, the identification of the enzymatic activities and the corresponding genes involved in this pathway has proven elusive. Thus, although a cytosolic indole synthase potentially involved in the conversion of indole-3-glycerol phosphate (IGP) into indole has been identified (Li et al. 1995; Ouyang et al. 2000; Wang et al. 2015), the mechanisms by which indole would then be converted into IAA and the overall relevance of this pathway remain controversial (Nonhebel 2015). In addition to the disputed TRP-independent pathway, several somewhat interconnected TRP-dependent routes for IAA production in plants have been proposed (Fig. 1), each with different levels of experimental support and scientific community acceptance (Nonhebel 2015). These TRP-dependent pathways are typically referred to by the name of a key biosynthetic intermediate.

The best characterized of these TRP-dependent routes of auxin production is the indole-3-pyruvic acid (IPyA) pathway that involves the conversion of TRP into IPyA by a small family of aminotransferases (TRP AMINOTRANSFERASE OF ARABIDOSPIS1 (TAA1) and TAA1-RELATED (TARs)) and IPyA into IAA by a family of flavin-containing monooxygenases (YUCCAs). Evidence in support of this pathway is, by far, the most conclusive and includes genetic, metabolic, and phylogenetic results that together

Received June 03, 2025. Accepted August 20, 2025.

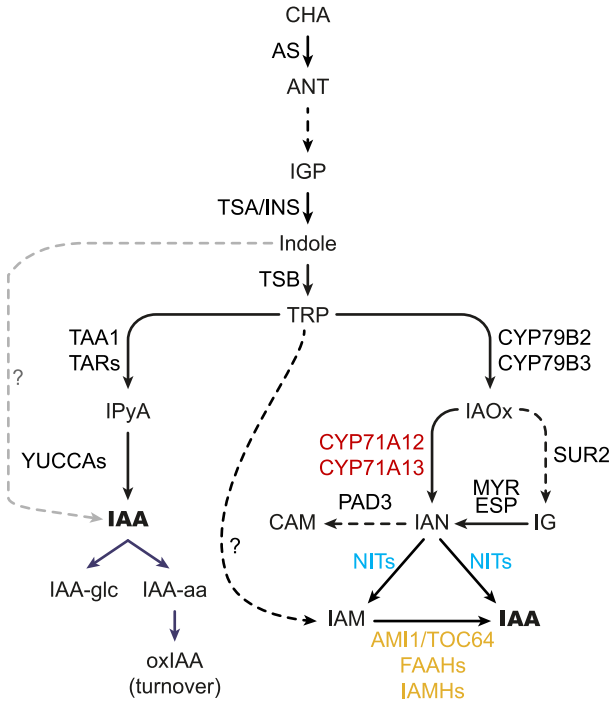

Figure 1. A model of the auxin biosynthesis pathway leading to the production of indole-acetic acid (IAA). Tryptophan (TRP)-dependent and TRP-independent routes are marked with black and gray arrows, respectively. Solid arrows indicate single-step conversions, while dashed arrows represent multistep conversions. TRP-dependent indole-pyruvic acid (IPyA) and putative indole acetaldoxime (IAOx) routes are depicted, as are the abbreviated versions of the upstream TRP biosynthesis out of chorismic acid (CHA) and the competing parallel indole glucosinolate (IG) and camalexin (CAM) biosynthesis routes that split at IAOx and indole-3-acetonitrile (IAN), respectively. The CYP71A, NIT, and AMI1/TOC64/FAAH protein families examined in this work as putative components of the IAOx pathway are displayed in red, blue, and yellow, respectively. CHA: chorismic acid, ANT: anthranilate, IGP: indole-3-glycerol phosphate, IAA-glc: glucose-conjugated IAA, IAA-aa: amino-acid-conjugated IAA (e.g. indole-3-acetyl-aspartate (IAA-Asp) and indole-3-acetyl-glutamate (IAA-Glu)), oxIAA: 2-oxindole-3-acetic acid, IAM: indole-3-acetamide; AS: anthranilate synthase, TSA: TRP SYNTHASE α (chloroplast), INS: INDOLE SYNTHASE (cytosol), TSB: TRP SYNTHASE β, TAA1: TRP AMINOTRANSFERASE OF ARABIDOPSIS1 (WEI8), TAR: TAA1-RELATED (TAR1, TAR2), NIT: NITRILASE (NIT1-NIT4), AMI1: AMIDASE1 (TOC64-I), TOC64: TRANSLOCON OF OUTER MEMBRANE OF THE CHLOROPLAST64 (*TOC64-III*, *TOC64-V*), FAAH: FATTY ACID AMIDE HYDROLASE (FAAH1-FAAH4), IAMH: IAM HYDROLASE (IAMH1, IAMH2), MYR: MYROSINASE, ESP: EPITHIOSPECIFIER PROTEIN, PAD3: PHYTOALEXIN DEFICIENT3, ?: unknown enzyme(s).

substantiate the universality and preponderance of this route among plants (Zhao et al. 2001; Stepanova et al. 2008, 2011; Tao et al. 2008; Yamada et al. 2009; Zhou et al. 2011; Eklund et al. 2015). In contrast, the experimental support for the rest of TRP-dependent pathways is somewhat fragmentary and inconclusive. For instance, although radiolabeled precursor feeding experiments indicate that key components of these other pathways —such as indole-3-acetaldoxime (IAOx), indole-3-acetonitrile (IAN), indole-3-acetamide (IAM), tryptamine (TAM), and indole-3-acetaldehyde (IAAld)—can all serve as intermediates in the production of IAA from TRP (Seo et al. 1998; Pollmann et al. 2002, 2006; Sugawara et al. 2009; Lehmann et al. 2010; Novák et al. 2012), conclusive identification of the enzymatic reactions and genes involved, and importantly, evidence supporting the physiological relevance of these pathways, are rather limited.

Support for the role of IAN as a TRP-derived IAA precursor comes not only from the radiolabeling experiments mentioned above but also from experimental evidence that a number of phylogenetically distant species have the ability to convert exogenous IAN into IAA (Thimann and Mahadevan 1964). Endogenous IAN has been reported for species belonging to the *Brassicaceae* family, like cabbage (*Brassica oleracea*) or *Arabidopsis* (Henbest et al. 1953; Rajagopal and Larsen 1972; Sugawara et al. 2009), but also in other species belonging to *Amaranthaceae*, *Asteraceae/Compositae*, *Convolvulaceae*, *Cucurbitaceae*, *Lamiaceae/Labiatae*, *Fabaceae/Leguminosae*, *Araceae/Lemnaceae*, or *Liliaceae* families (Rajagopal and Larsen 1972) and in coleoptiles of monocots (*Poaceae/Gramineae*) like maize and oat (*Avena sativa*) (Rajagopal and Larsen 1972; Park et al. 2003). The identification of a set of *Arabidopsis* mutants impaired in their response to exogenous IAN shed more light on the potential role of IAN as an auxin precursor (Normanly et al. 1997). Characterization of these mutants identified *NITRILASE1* (*NIT1*) as a gene involved in the plant response to exogenous IAN. *NIT1* is a member of a small family of 4 genes in *Arabidopsis*, *NIT1* through *NIT4*, of which *NIT1* to *NIT3* are thought to function in IAN metabolism, whereas *NIT4* has been implicated in cyanide detoxification (Vorwerk et al. 2001; Mulelu et al. 2019). Although *NIT1* to *NIT3* can convert IAN into IAA in vitro, they show much greater affinity and catalytic rate transforming other naturally occurring substrates, like 3-phenylpropionitrile, allyl cyanide, (phenylthio)acetonitrile, or (methylthio)acetonitrile, than they do for IAN (Vorwerk et al. 2001). Importantly, neither the loss of function of *NIT1* nor the knockdown RNAi lines for *NIT1* to *NIT3* showed obvious phenotypic defects beyond the resistance to exogenous IAN (Normanly et al. 1997; Lehmann et al. 2017), casting some doubts about the role of endogenous IAN as an IAA precursor and the potential physiological relevance of a native IAN-dependent IAA biosynthetic pathway. Nevertheless, due to functional redundancy among the *NIT* gene family members and the potential residual gene activity in the RNAi knockdowns, the lack of obvious phenotypes of these mutants has not formally ruled out a potential role of this gene family in the production of IAA during normal plant development.

As with IAN, a variety of plant species have been shown to contain IAM (Pollmann et al. 2003, 2006; Lehmann et al. 2010) and to have the capability of uptaking exogenous IAM and converting it into IAA (Pollmann et al. 2003, 2006; Lehmann et al. 2010). The isolation and characterization of AMIDASE1 (AMI1), an *Arabidopsis* amidase capable of hydrolyzing IAM in vitro (Pollmann et al. 2003, 2006), along with its paralogs from the most-closely related *TRANSLOCON OF THE OUTER MEMBRANE OF THE CHLOROPLASTS64* (*TOC64*) gene family (*TOC64-III* and *TOC64-V*; Pollmann et al. 2006; Aronsson et al. 2007) and a more distantly related *FATTY ACID AMIDE HYDROLASE* (*FAAH*) family (Pollmann et al. 2006; Keereetaweep et al. 2013), provided an opportunity for testing the potential role of the IAM pathway in plants. As in the case of the *NIT*s, the lack of a systematic mutant analysis of *AMI1* and related genes has precluded the conclusive placement of these genes in a hypothetical IAM route of auxin biosynthesis. More recently, an *IAM HYDROLASE* (*IAMH1*), unrelated in sequence to *AMI1*, was identified in *Arabidopsis* using genetic screening for IAM-resistant mutants and implicated in the conversion of IAM to IAA (Gao et al. 2020). *IAMH1* has a close paralog in *Arabidopsis*, *IAMH2*, that, based on double-mutant analysis, is also involved in the production of IAA in plants treated with IAM. Importantly, although these double-mutant plants show clear resistance to exogenous IAM, they do not display prominent auxin-related developmental defects under normal

laboratory growth conditions (Gao et al. 2020), questioning their role in the proposed IAM-dependent IAA biosynthetic pathway.

In contrast with IAM, IAOx has only been detected in some plant species belonging to the *Brassicaceae* family (Cooney and Nonhebel 1991; Sugawara et al. 2009) and in 2 species of the genus *Erythroxylum* (*Erythroxylaceae*; Luck et al. 2016). Consistent with this, the presence of close homologs of the *Arabidopsis CYP79B* gene family involved in the conversion of TRP to IAOx has also been found only in the Brassicales order (Bak et al. 2001). In these plant species, IAOx is a precursor in the production of 2 defense compounds: indole glucosinolates (IGs; Bak et al. 1998, 2001; Hull et al. 2000; Mikkelsen et al. 2000; Zhao et al. 2002) and camalexins (CAM; Glawischnig et al. 2004; Nafisi et al. 2007; Müller et al. 2015). Importantly, several enzymatic reactions and the corresponding genes involved in these 2 pathways have been identified and characterized in *Arabidopsis*. Thus, the first step in the IG pathway consists of the conversion of TRP into IAOx by 2 partially redundant cytochrome P450s, CYP79B2 and CYP79B3 (Hull et al. 2000; Mikkelsen et al. 2000; Zhao et al. 2002), a step that is shared with the CAM biosynthesis pathway (Glawischnig et al. 2004). Accordingly, the *cyp79b2 cyp79b3* double mutant completely lacks these 2 important defense compounds (Glawischnig et al. 2004). IAOx can then be channeled into the production of CAM by a small family of cytochrome P450s related to CYP71A13 (Nafisi et al. 2007; Müller et al. 2015) or into IG by CYP83B1 (SUPERROOT2, SUR2) (Bak et al. 2001). Like the conversion of TRP into IAOx by the CYP79B2/3, the mutant analysis provides strong support for the involvement of SUR2 and CYP71A12/13 in the first committed steps of IG and CAM biosynthesis, respectively, as the production of these defense compounds was greatly reduced in the corresponding mutants (Zhao et al. 2002; Nafisi et al. 2007; Müller et al. 2015).

The connection of CAM and IAA biosynthesis pathways stems from the involvement of IAN as the product of IAOx dehydration catalyzed by CYP71A12/13 (Mucha et al. 2019). On the other hand, the link between IG and IAA biosynthesis comes from the high-auxin phenotypes observed not only in the *sur2* mutant but also in several of the mutants affecting downstream IG pathway genes such as *SUR1* (Boerjan et al. 1995) and *UDP-GLUCOSYLTRANSFERASE 74B1* (*UGT74B1*) (Grubb et al. 2004). Furthermore, feeding experiments using radiolabeled IAOx in the *cyp79b2 cyp79b3* mutant identified IAN and IAM as likely conversion products of IAOx (Sugawara et al. 2009). These results, together with the current understanding of the role of *CYP71As*, *NITs*, *AMI*, and *IAMHs* in the metabolism of IAOx, IAN, and IAM, respectively, have been used to propose a metabolic and genetic pathway for the production of IAA from IAOx (Sugawara et al. 2009). In this pathway, IAOx would be first converted into IAN by the CYP71As, NITs would then catalyze the conversion of IAN into IAM and/or IAA, and finally, AMI and/or IAMH would catalyze the formation of IAA from IAM (Fig. 1).

The IAOx pathway has attracted considerable attention due to the fact that its activation in *sur2* and other IG mutants results in plants with high IAA levels and strong auxin overproduction phenotypes (Boerjan et al. 1995; Seo et al. 1998; Barlier et al. 2000; Grubb et al. 2004), suggesting a potential physiologically relevant alternative to the IPyA pathway of IAA production. On the other hand, the general importance of the IAOx route of auxin production is somewhat diminished by its restriction to mostly plant species of the *Brassicaceae* family and the lack of prominent developmental defects in the *cyp79b2 cyp79b3* double-knockout mutants where this pathway is completely blocked (Stepanova et al. 2011; Tsugafune et al. 2017). It is important to emphasize, however, that plants as distantly related to *Arabidopsis* as maize have been shown to contain the enzymatic machinery necessary to convert exogenous IAOx into IAA (Perez et al. 2021), and *Medicago truncatula* plants treated with IAOx show strong high-auxin phenotypic responses (Buezo et al. 2019; Roman et al. 2023). Furthermore, although no homologous sequence to *CYP79B2* or *CYP79B3* can be found in the maize genome, cytochrome P450s of the CYP79A family have been shown to be able to produce IAOx and phenyl-acetaldoxime (PAOx) in maize and sorghum, respectively (Irmisch et al. 2015; Perez et al. 2023), leaving open the possibility for a functional IAOx-related pathway in a broader range of plant species.

Thus, the current view of the IAA production pathways that may function in plants in parallel with the primary IPyA-dependent route is confusing, with different levels of support and undermining experimental evidence having been put forward. One key limitation to addressing this problem has been the lack of mutant lines where the whole family of genes putatively involved in these alternative IAA production pathways has been knocked out. Thus, as the first step toward clarifying the role of the different IAA biosynthetic pathways, we generated high-order mutant lines for each of 3 key gene families, *CYP71A12/13/18*, *NIT1/2/3/4*, and *AMI1/TOC64/FAAH*, that in combination with previously characterized mutants (such as *sur2*, *cyp79b2 cyp79b3*, and *iamh1 iamh2*) and a comprehensive set of phenotypic and metabolic approaches have allowed us to thoroughly test the role of these gene families in auxin biosynthesis. Our results clearly indicate that none of the 3 gene families investigated here play a role in the IAOx pathway activated in the *sur2* mutant and question the validity of the previously proposed linear pathway for the conversion of IAOx into IAA via IAN and IAM. We anticipate this work will trigger new efforts to unveil how excess auxin is produced in *sur2* and investigate the possible physiological relevance of such a pathway in *Brassicaceae* and beyond.

Results

Generation of mutant lines

In addition to the predominant IPyA auxin biosynthetic pathway, a second TRP-dependent route to produce IAA via IAOx, IAN, and IAM has been proposed in *Arabidopsis* and other *Brassicaceae* species (Fig. 1) (Sugawara et al. 2009). The enzymes thought to catalyze the corresponding reactions are encoded by 3 multigenic families represented in *Arabidopsis* by the *CYP71As* (Nafisi et al. 2007; Müller et al. 2015), *NITs* (Normanly et al. 1997), and *AMIs* (Lehmann et al. 2010). Although several lines of evidence support individual steps of this metabolic pathway as described above, the possible connections between the individual steps and the overall functionality of this pathway have not been thoroughly investigated. Thus, in order to test the potential contribution of the proposed IAOx-dependent pathway to the IAA pools in *Arabidopsis*, we decided to take a genetic approach and examine the phenotypic and metabolic consequences of knocking out the 3 enzymatic steps mentioned above. Due to potential functional redundancy, we first identified the closest family members of the 3 better-characterized enzymes in the IAOx pathway: *CYP71A13*, *NIT1*, and *AMI1*. Amino acid sequence comparison and phylogenetic analysis (Supplementary Fig. S1) led us to identify 3 genes as part of the CYP71A family (*A12*, *A13*, and *A18*), 4 members in the *NIT* family (*NIT1-NIT4*), and consistent with previous reports, 7 extended *AMI* family members that include 3 *TOC64*s and 4 *FAAH*s (Pollmann et al. 2006) potentially involved in IAOx-dependent auxin biosynthesis.

To test the involvement of these 3 gene families in IAA production, we used a combination of publicly available T-DNA lines and targeted genomic editing tools to generate the corresponding

high-order gene family mutants (Supplementary Figs. S2 and S3). We observed embryo lethality in *faah3* single mutants (Supplementary Fig. S4), and therefore, the highest-order mutant for the *AMI* gene family was propagated as a segregating line, *ami1-1 toc64-III toc64-V faah1 faah2 faah3/+ faah4*. The knockouts for the whole *CYP71A* and *NIT* families were fully viable and fertile under standard laboratory control conditions. Considering the strong phenotype described for the IPyA-deficient *TAA1/TAR* family *wei8 tar2* double mutant and the early development arrest of *wei8 tar1 tar2* triple mutant (Stepanova et al. 2008), we hypothesized that the contribution of the IAOx pathway to the auxin pools in plants grown under standard laboratory conditions would be, at best, minor. Therefore, to enhance any potential auxin-related phenotypes that plants lacking functional *CYP71A*, *NIT*, and *AMI1/TOC64/FAAH* gene families may have, we genetically activated the metabolic flux of the proposed IAOx pathway by introgressing the *sur2* T-DNA allele (Stepanova et al. 2005) into the 3 high-order gene family knockout lines mentioned above. Due to difficulties in combining the existing mutant alleles of *faah4* and *sur2* because of genetic linkage, the fairly distant phylogenetic relationship between the founding family member AMI1 and FAAH4 (Supplementary Fig. S1), and the embryo lethality of *faah3* (Supplementary Fig. S4), the highest-order mutant for the *AMI* family in the *sur2* background we built was *ami1-2 toc64-III toc64-V faah1 faah2 sur2*. Then, to determine the potential involvement of these 3 gene families in auxin production in the wild type (WT), as well as in the *sur2* mutant background, we carried out a battery of phenotypic and metabolomic analyses of the higher-order mutants of each gene family with and without *sur2*. We reasoned that the role of individual genes could be dissected at a later stage once a specific phenotype was observed for the high-order mutants, hereon referred to as IAOx high-order mutants.

Mutants with defects in the postulated IAOx pathway do not show auxin-related defects and fail to suppress high-auxin phenotypes of *sur2*

To determine the potential involvement of *CYP71A*, *NIT*, and *AMI1/TOC64/FAAH* gene families in auxin biosynthesis, we examined a battery of auxin-related phenotypes of their high-order mutants using the mild auxin-deficient *wei8-1* mutant (Stepanova et al. 2008; Tao et al. 2008; Yamada et al. 2009) as a positive control for subtle auxin-related defects (Fig. 2A; Supplementary Fig. S5, A to D). Considering the heterogeneity in age and growth conditions utilized in the literature to characterize auxin-related phenotypes in seedlings, we examined growth and development in our set of mutants under multiple setups—3 d in continuous darkness, 7 d in continuous light, or 3 d in the dark followed by a 4-d continuous light treatment—to enable comparisons of the phenotypes of these mutants with that of their published predecessors. The mild auxin-deficient *wei8* mutant did not display any major developmental defects in seedling organ size (hypocotyl and root length) when grown in constant darkness (3 d; Supplementary Fig. S5, A and C) or under continuous light (7 d; Supplementary Fig. S5, B and D). However, *wei8* roots were significantly shorter than those of WT when 3-d-old dark-grown seedlings were transferred to continuous light for 4 additional days (Fig. 2, A and C; Supplementary Data Set 1). In contrast, none of the high-order IAOx mutants showed significant differences in seedling organ size compared to WT under any of the growth conditions tested (Fig. 2, B and C; Supplementary Fig. S5, A to D and Supplementary Data Set 1). Furthermore, neither *wei8* nor IAOx mutants displayed any prominent phenotypic defects in soil-grown adults under standard laboratory control conditions (Fig. 2D; Supplementary Data Set 1).

Given the absence of observable defects in high-order IAOx mutants, including the previously characterized *cyp79b2 cyp79b3* known to block the production of IAOx from TRP (Stepanova et al. 2011) (Fig. 2), we considered the possibility that the IAOx pathway may not be active at the developmental stages or under the environmental conditions examined. Therefore, we characterized the phenotypes of these mutants when the putative IAOx pathway is genetically activated by knocking out the *SUR2* gene. In this mutant, the flow of IAOx into IG production is blocked, with IAOx now channeled into IAA production (Fig. 1) (Barlier et al. 2000; Bak et al. 2001). Overproduction of auxin in *sur2* translated into statistically shorter hypocotyls and roots in 3-d-old dark-grown seedlings (Supplementary Fig. S5, A and C; Supplementary Data Set 1) or longer hypocotyls and shorter roots in 7-d-old plants grown in constant light (Supplementary Fig. S5, B and D; Supplementary Data Set 1) or in the dark for 3 d followed by 4 d in the light (Fig. 2, A to C; Supplementary Data Set 1). Additionally, high levels of auxin in *sur2* plants led to the development of characteristic small, epinastic cotyledons (Fig. 2A) and the disintegration of hypocotyls upon adventitious root emergence in 7-d-old seedlings that underwent a dark-to-light transition (Fig. 2E), as well as small, epinastic rosette leaves in soil-grown adults (Fig. 2D). As expected, *wei8* did not suppress any of the high-auxin phenotypes of *sur2* (Fig. 2; Supplementary Fig. S5; Supplementary Data Set 1) since *WEI8* and *SUR2* are thought to take part in 2 independent auxin biosynthesis routes. On the other hand, we reasoned that if indeed the IAOx gene families studied in this work were involved in the proposed IAOx-dependent *sur2*-activated auxin biosynthesis pathway, knocking them out should result in the suppression of the *sur2* high-auxin phenotype, as observed in the *cyp79b2/b3 sur2* triple mutant in all the growth conditions tested (Fig. 2; Supplementary Fig. S5; Supplementary Data Set 1) (Stepanova et al. 2011). However, none of the IAOx family mutants suppressed any of the *sur2* phenotypes examined above, neither at the seedling stage (Fig. 2, A to C; Supplementary Fig. S5; Supplementary Data Set 1) nor at the 3-wk-old rosette stage, under standard laboratory control conditions (Fig. 2D).

We looked into the possibility that the T-DNA intronic mutant alleles could be spliced out, with the functionality of the gene fully restored. We found that the expression of *AMI1* in the *ami1-1 toc64-III toc64-V faah1 faah2 faah3/+ faah4* mutant was reduced more than 330-fold compared to WT, whereas the levels of *FAAH1* and *FAAH4* were mildly reduced (Supplementary Fig. S6; Supplementary Data Set 1). As all other *CYP71A*, *NIT*, and *AMI1/TOC64* mutants leveraged in this work are exonic knockouts or deletions (Supplementary Fig. S2), in the absence of prominent phenotypes, we conclude that (1) the most closely related members of these gene families examined herein do not play a prominent role in auxin biosynthesis under the studied growth conditions and (2) their functions are not required for the auxin production activated in *sur2* mutant plants.

The currently accepted metabolic pathway for the conversion of IAOx to IAA needs to be reassessed

The inability of the high-order IAOx mutants to suppress the *sur2* high-auxin phenotypes suggests that the corresponding enzymes may not be involved in the sequential conversion of IAOx into IAN, IAM, and finally, IAA (Fig. 1). Alternatively, these protein families may catalyze the proposed enzymatic reactions, but the

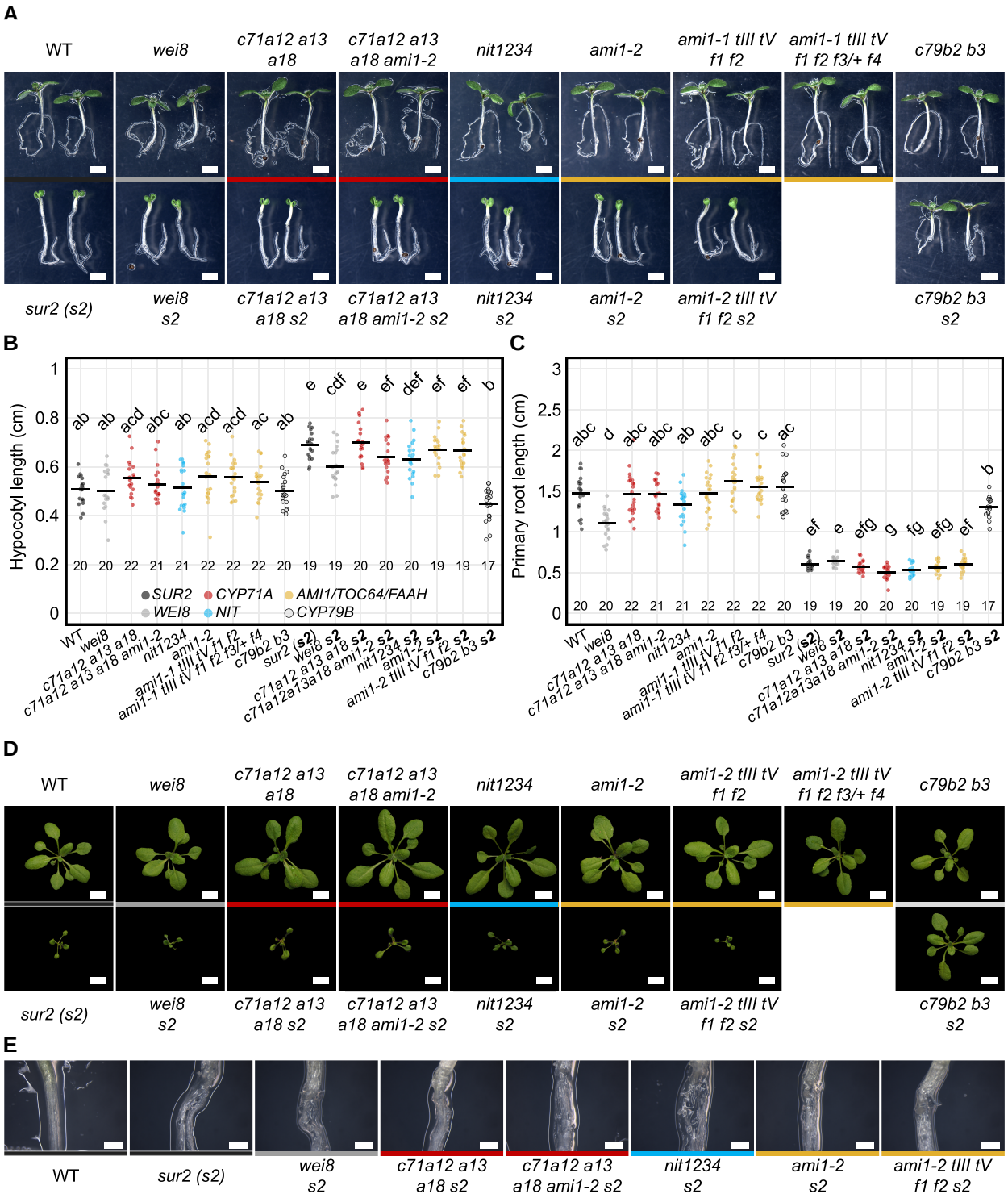

Figure 2. Mutants defective in the proposed IAOx pathway of auxin biosynthesis display no prominent growth defects. **A)** Phenotypes of seedlings germinated on horizontal plates in the dark for 3 d and transferred to continuous light for 4 additional days. Scale bar = 2 mm. Background marks with spatial consistency nearby the seedlings are scratches of the equipment's base. **B**, **C)** Organ size measurement and statistical analysis of seedlings shown in (A). Horizontal bars represent the mean values for each genotype for a given organ. Different letters denote statistically significant differences analyzed by ANOVA for $\alpha = 0.05$. The numbers below the datapoints indicate the sample size for a given genotype. More details of statistical analyses results are available in Supplementary Data Set 1. **D)** Rosettes of 3-wk-old plants grown in soil under long-day conditions (16-h fluorescent light/8-h darkness) after germination on vertical plates for 3 d in the dark and 4 d under continuous LED light. Images were digitally extracted for comparison. Scale bar = 1 cm. **E)** The characteristic high-auxin hypocotyl disintegration phenotype of 7-d-old *sur2* seedlings grown for 3 d in the dark followed by 4 d in continuous light is not prevented by mutations in genes implicated in the putative IAOx pathway. Scale bar = 2 mm. Genotypes in WT or *sur2* background are color-coded by the mutated gene family. From left to right: black (*SUR2*: WT and *sur2*), dark gray (*WEI8*: *wei8* and *wei8 sur2*), red (*CYP71A*: *c71a12a13a18*, *c71a12a13a18 ami1-2*, *c71a12a13a18 s2*, *c71a12a13a18 ami1-2 s2*), blue (*NIT*: *nit1234* and nit1234 s2), yellow (*AMI1/TOC64/FAAH*: *ami1-2*, *ami1-1 tIII tV f1 f2*, *ami1-1 tIII tV f1 f2 f3/+ f4*, *ami1-2 s2*, *ami1-1 tIII tV f1 f2 s2*), light gray and black border (*CYP79B*: *c79b2b3*, *c79b2b3 s2*). WT: wild type (Col-0), *c71a12 a13 a18*: *cyp71a12 cyp71a13 cyp71a18*, *c71a12 a13 a18 ami1-2*: *cyp71a12 cyp71a13 cyp71a18 ami1-2*, *nit1234*: *nit1 nit2 nit3 nit4*, *ami1-1 tIII tV f1 f2*: *ami1-1 toc64-III toc64-V faah1 faah2*, *ami1-1 tIII tV f1 f2 f3/+ f4*: *ami1-1 toc64-III toc64-V faah1 faah2 faah3/+ faah4*, *s2*: *sur2*, *c79b2 b3*: *cyp79b2 cyp79b3*.

metabolic pathway by which excess auxin is produced in *sur2* is different from the previously postulated IAOx–IAN–IAM–IAA route (Sugawara et al. 2009). To clarify this situation, we decided to examine the effects of feeding various auxin precursors and the ability of the different high-order IAOx mutants to block the potential phenotypic consequences of the conversion of these auxin precursors into IAA in planta.

To determine the experimental conditions where these compounds trigger clear auxin-like responses, we first examined the auxin-related phenotypes of increasing concentrations of each of the proposed IAA precursors of the IAOx pathway in WT plants in 3-d-old dark-grown (Supplementary Fig. S7) and 5-d-old light-grown plants (Fig. 3; Supplementary Fig. S7). We observed that in both experimental setups, exogenous IAOx and IAN, much like with IAA treatments, led to prominent dose-dependent root growth inhibition in WT plants, whereas IAM treatment led to profound hypocotyl growth promotion specifically in the light (Fig. 3; Supplementary Fig. S7). In 3-d-old dark-grown WT seedlings exposed to high IAM concentrations of 20 µM and above, mildly shorter root and hypocotyl lengths were observed relative to plants exposed to the solvent (DMSO) (Supplementary Fig. S7). In contrast, in continuous light, 10–60 µM IAM stimulated pronounced (1.5–3-fold) hypocotyl elongation in 5-d-old WT seedlings, whereas the root lengths of these plants were inhibited at 20 µM IAM and above by up to 25% (Fig. 3).

To determine if these phenotypic changes were indeed due to an increase in IAA activity in the treated plants, we examined the effects of these putative auxin intermediates in *aux1-7*, a mutant impaired in the cellular import of IAA and, therefore, compromised in the cell-to-cell movement of this hormone (Pickett et al. 1990; Bennett et al. 1996; Marchant et al. 1999). We found that *aux1* showed partial insensitivity to all precursors (Fig. 3; Supplementary Fig. S7), suggesting that the phenotypes observed in WT plants treated with these compounds were, at least to some extent, due to the conversion of these precursors into IAA.

To further verify that the phenotypes observed in WT plants upon exogenous application of these putative IAA precursors were indeed associated with an increase in auxin responses, we examined the activity of the auxin reporter *DR5:GFP* (Fig. 4). Three-day-old, etiolated WT seedlings harboring this transcriptional auxin response sensor showed higher *DR5* reporter activity in root tips and root–hypocotyl junctions of plants exposed to IAOx or IAN. Elevated *DR5* activity was also observed in the apical hooks in the presence of all 3 compounds, with the IAN- and IAM-treated plants also showing partially open hooks concomitant with an especially high activity of *DR5* in these tissues (Fig. 4A). When seeds were germinated and grown under continuous light for 5 d, IAOx-treated plants recapitulated the patterns observed in IAA-treated plants, i.e. shorter roots with strong *DR5* activity in the proximal region of the root and root–hypocotyl junction, with a milder induction in the aerial parts (Fig. 4B). Although we observed a prominent activation of *DR5* in the aerial parts of both IAN- and IAM-treated seedlings, each compound had different phenotypic signatures. Thus, IAN-treated plants showed shorter roots but no effects on hypocotyl elongation or leaf epinasty, whereas IAM treatment had no effect on roots but dramatically promoted hypocotyl elongation and leaf epinasty (Fig. 4B).

To rule out the possibility that an apparent increase in *DR5* activity was an artifact due to the smaller size of the organs observed in some treatments, we examined the effects of these compounds on *DR5* activity after a shorter (16-h) exposure when the phenotypic effects of these treatments on organ size were less prominent (Supplementary Fig. S8). Consistent with what was observed with the longer treatments, 16 h post transfer of 3-d-old, etiolated seedlings to plates containing IAOx or IAN resulted in an increase in *DR5* activity in the roots, while the effects of the IAM treatment were again restricted to the hypocotyls and cotyledons of dark-grown seedlings. Similarly, 16 h after the transfer of 5-d-old light-grown seedlings to precursor-supplemented plates, we observed an increase in *DR5* activity in the roots of IAOx- and IAN-treated plants and in the hypocotyls and cotyledons of IAM-treated seedlings. These results support the idea that the auxin-related phenotypes triggered by these compounds are indeed due to their conversion into active IAA. Interestingly, each one of these compounds had certain tissue specificity, with IAOx having an effect predominantly in underground tissue (roots), IAM predominantly affecting aboveground tissues (hypocotyls and cotyledons), and IAN acting in both hypocotyls and roots (Fig. 4B, Supplementary Fig. S8).

To determine whether or not the conversion of these compounds into IAA requires the activity of the 3 enzyme families studied here, we examined the phenotypic effects of these compounds in high-order mutants for each of the 3 gene families in both 5-d-old light-grown (Fig. 3) and 3-d-old dark-grown seedlings (Supplementary Fig. S5). Phenotypic analysis of high-order mutants of the *CYP71A* and *AMI1/TOC64/FAAH* families showed that the response of these mutants to IAOx, IAN, and IAM was not significantly different than that of WT under all of the growth conditions examined (Fig. 3; Supplementary Fig. S7). The inability of these high-order mutants to suppress the auxin-like effects of treatments with the proposed IAOx pathway intermediates argues against the previously proposed involvement of these gene families in the conversion of these compounds into IAA in planta. In contrast, and as expected from previous work using the single *nit1-3* mutant (Normanly et al. 1997), the roots of the *nit1234* quadruple mutant showed clear insensitivity to the IAN treatment (Fig. 3; Supplementary Fig. S7). These results, together with the fact that *nit1234* does not show a consistently altered response to IAA (Supplementary Fig. S7; Supplementary Fig. S9), strongly support the idea that the nitrilase activity is required for the conversion of IAN taken up by the plant into IAA. Furthermore, the profound root insensitivity to IAN observed in *aux1* (Fig. 3; Supplementary Fig. S7) is most likely due to the impaired cell-to-cell IAA transport rather than to a putative disruption of the IAN uptake capacities of this mutant, although we have not formally ruled out the latter possibility. Finally, the fact that the *nit1234* responds normally to IAOx suggests that IAN is an unlikely intermediate in the direct conversion of IAOx taken up into IAA.

In addition to the amidase family described above, 2 IAM hydrolases, IAMH1 and IAMH2, have been recently implicated in the conversion of IAM into IAA in vivo (Gao et al. 2020). Consistent with prior reports, the increase in hypocotyl elongation of 5-d-old light-grown seedlings in response to IAM observed in WT plants was significantly attenuated in the *iamh1 iamh2* double mutant (Fig. 3). Interestingly, this double mutant responded normally to IAA and the other IAA precursors tested (Fig. 3; Supplementary Fig. S7). Following the same logic as used above to interpret the results of the IAN-treated *nit1234* mutant, we conclude that IAM is not a likely metabolic intermediate in the conversion of IAOx and IAN into IAA, as otherwise *iamh1 iamh2* should have been insensitive not only to the IAM but also to the IAOx and IAN supplementation. The lack of IAM insensitivity in *AMI* family mutants, unlike that of *iamh1 iamh2*, indicates that *AMI1/TOC64/FAAH* does not play a prominent role in transforming IAM into IAA in *Arabidopsis*, and this finding is consistent with the lack of suppression of the high-auxin phenotypes of

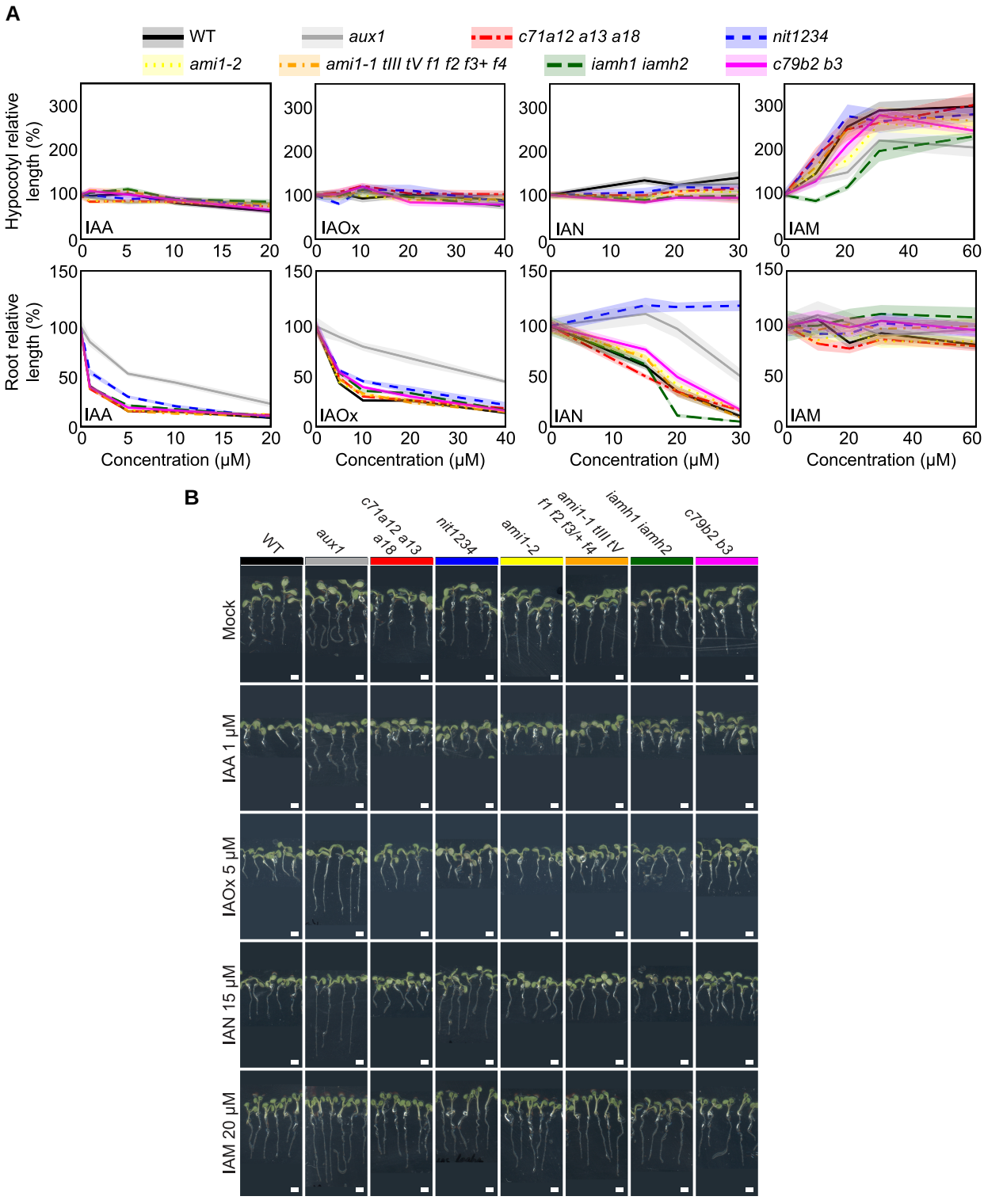

Figure 3. Phenotypes of light-grown mutants impaired in the putative IAOx route challenge the established model of the IAOx pathway. **A)** WT and mutant lines were germinated on horizontal plates under continuous light for 5 d in control media or in media supplemented with the indicated concentrations of IAA, IAOx, IAN, and IAM (Supplementary Table S4). For each treatment, the "0" concentration contains the equivalent concentration of DMSO as the highest concentration tested for a specific auxin precursor. Root and shoot lengths were measured in ImageJ. Relative organ size at a given concentration for a specific genotype was calculated by dividing the organ size by that in the corresponding control ([metabolite] = 0). Average relative organ sizes (lines) and confidence intervals (CI = 95%, shades) were plotted using R studio. **B)** Photographs of representative plants for one of the concentrations for each compound. A dark background similar to that in the original image was added underneath each picture to keep the image sizes uniform for aesthetic purposes. These precursor concentrations were chosen as they produce similar organ sizes in the WT as 1 μM IAA. Scale bar = 2 mm. WT: wild type (Col-0), *aux1: aux1-7*, *c71a12 a13 a18: cyp71a12 cyp71a13 cyp71a18*, *nit1234: nit1 nit2 nit3 nit4*, *ami1-1 tIII tV f1 f2 f3/+ f4: ami1-1 toc64-III toc64-V faah1 faah2 faah3/+ faah4*, *iamh1 iamh2: iamh1-1 iamh2-2*, *c79b2 b3: cyp79b2 cyp79b3*.

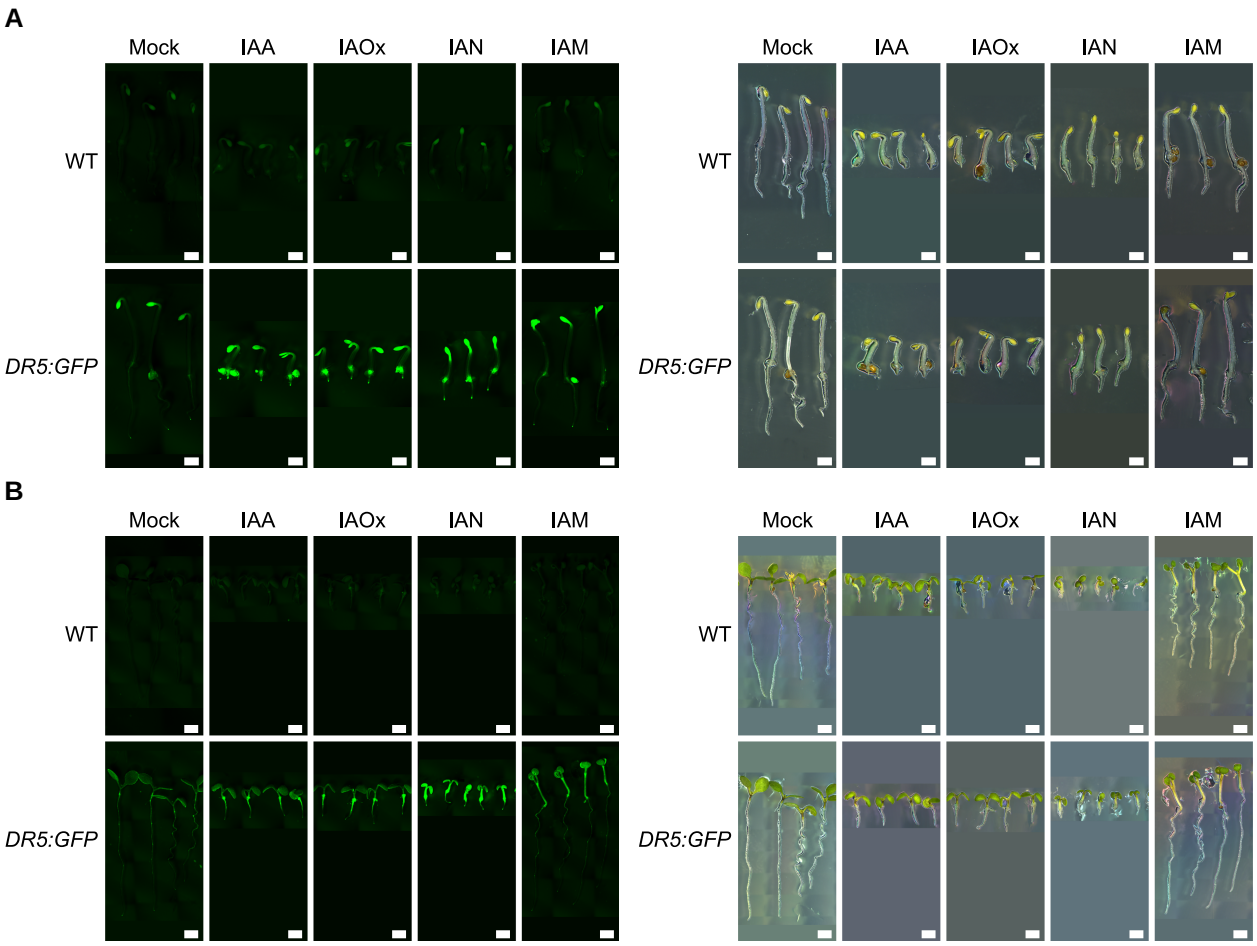

Figure 4. Putative IAOx route intermediates, IAOx, IAN, and IAM, induce *DR5:GFP* auxin reporter activity. **A**, **B)** Three-day-old dark-grown seedlings (A) and 5-d-old light-grown seedlings (B) were germinated on horizontal AT plates supplemented with the indicated auxin precursors at concentrations empirically determined to be the lowest for seedlings to reach maximum change in organ size (Fig. 3A). Dark experiment (A): 0.3 µM IAA, 5 µM IAOx, 20 µM IAN, 50 µM IAM. Scale bar = 1 mm. Light experiment (B): 3 µM IAA, 20 µM IAOx, 30 µM IAN, 50 µM IAM. All pictures in this figure are composite images, where individual images within a panel utilized the same imaging settings. A dark background similar to that in the original image was added underneath each picture to keep the image sizes uniform for aesthetic purposes. Scale bar = 2 mm.

sur2 by *ami1-2 toc64-III toc64-V faah1 faah2*. To test if the IAM insensitivity of *iamh1 iamh2* can suppress *sur2*, we introgressed *iamh1 iamh2* into the *sur2* background (Supplementary Fig. S10). Critically, the *iamh1 iamh2 sur2* triple mutant was phenotypically indistinguishable from *sur2* under standard laboratory control conditions, demonstrating that IAM-to-IAA conversion is not necessary for auxin overproduction in *sur2*.

Unlike the genetically supported NIT- and IAMH-mediated conversion of exogenous IAN and IAM, respectively, into IAA in plants, the lack of genetic evidence for the enzymatic conversion of IAOx into IAA made us wonder whether the auxin-like phenotypes observed in seedlings exposed to exogenous IAOx were caused by spontaneous conversion into IAA—as observed for the IAA precursor IPyA (Stepanova et al. 2008)—or by IAA impurities present in our IAOx stock. To test these possibilities, we first analyzed our laboratory's IAOx stocks by high-performance liquid chromatography (HPLC) coupled with electrospray ionization (ESI) and mass spectrometry (MS) (HPLC-ESI-MS). While both trans- and cis-isomers are present in our IAOx standard, no IAA was detected (Supplementary Fig. S11A). Next, we incubated an IAOx solution (10 ng/µL) in a growth chamber in the light or in the dark for 5 d, mimicking the experimental conditions used in our phenotyping studies. The LC-MS analysis of these samples showed no conversion of IAOx to IAA regardless of exposure to light (Supplementary Fig. S11B). Therefore, we conclude that the phenotypes observed upon exogenous supplementation of plant growth media with IAOx could not be the consequence of the spontaneous formation of IAA from IAOx in vitro.

In summary, our results presented in this section are consistent with the previously proposed idea that IAOx, IAN, and IAM can function as IAA precursors when exogenously provided to plants in the media. They also support the prevalent view that nitrilases and IAM hydrolases play a role in the in vivo conversion of exogenously applied IAN and IAM into IAA, respectively. On the other hand, our work questions the existence of the proposed IAOx→IAN→IAM→IAA linear metabolic pathway and the involvement of IAN and IAM as intermediates in the excess auxin production observed in the *sur2* mutant. Our findings instead suggest that each of the 3 postulated auxin precursors—IAOx, IAN, and IAM—follows an independent route to become an active auxin. Importantly, although NITs and IAMHs are promising enzymes for converting IAN and IAM, respectively, into IAA, no suitable enzyme candidate exists for the transformation of IAOx into IAA in vivo. Future genetic and metabolic analysis of *sur2* would be essential for identifying genes coding for such enzymes.

Mutants in the postulated IAOx pathway do not display prominent auxin defects in classical auxin-related phenotypic assays

The results described so far indicate that the functions of the 3 gene families examined in this work (*CYP71A*, *NIT*, and *AMI*) and the *IAMH* family are not required for the excess production of auxin in the *sur2* mutant, nor for normal plant development under standard laboratory growth conditions. This, however, does not rule out the possibility that these genes may participate in the production of auxin under specific growth conditions where a burst of auxin production is required. In fact, *TAA1*, a central component of the IPyA auxin biosynthetic pathway, was originally identified not because of any prominent general developmental defect of the corresponding mutant but due to its altered ethylene (Stepanova et al. 2008) and shade avoidance (Tao et al. 2008) responses, phenotypes that rely on a local increase in auxin production. Thus, we reasoned that to uncover any potential role of the *CYP71A*, *NIT*, and *AMI* gene families in auxin biosynthesis, the performance of the corresponding high-order mutants should be examined in a battery of phenotypic assays highly sensitive to alterations in the auxin biosynthesis, transport, or signaling pathways. Thus, we first examined the root and hypocotyl sensitivity of the high-order IAOx mutants to the ethylene precursor 1-aminocyclopropane-1-carboxylic acid (ACC) (Merchante and Stepanova 2017) as it is well known that even mild alterations in the production, transport, or sensitivity to auxin result in a significant reduction in the ACC-triggered growth inhibition. As previously reported (Stepanova et al. 2008), the ACC response of *wei8*, a weak auxin biosynthetic mutant defective in *TAA1*, was normal in the hypocotyls of 3-d-old etiolated seedlings but significantly reduced in the roots (Fig. 5A; Supplementary Data Set 1). Furthermore, *sur2* showed WT level of root sensitivity to ACC, whereas *wei8 sur2* presented an intermediate phenotype, suggesting that production of *sur2*-mediated excess auxin can partially compensate for *wei8*'s deficit in this hormone. Interestingly, none of the high-order IAOx mutants showed any major defects in ACC sensitivity, and the mild phenotypes initially observed in the *cyp71a12/13/18 sur2* hypocotyls and *nit1/2/3/4 sur2* roots were not reproducible across multiple experimental repetitions (Supplementary Fig. S12; Supplementary Data Set 1) and are thus likely not biologically relevant.

In addition to the altered response to ACC, another hallmark of auxin deficiency is the alteration of gravitropic responses, as previously reported for auxin biosynthesis (*wei8 tar2*, Stepanova et al. 2008), transport (*aux1*, Pickett et al. 1990; Bennett et al. 1996; Marchant et al. 1999), and signaling (*tir1*, Hobbie and Estelle 1994; Ruegger et al. 1998) mutants. Thus, to further explore the possible roles of the gene families postulated to be involved in IAOx-dependent auxin biosynthesis, we examined the root vertical growth index (VGI) as a sensitive measure of gravity responses in both dark- and light-grown seedlings (Marchant et al. 1999; Rahman et al. 2001; Grabov et al. 2005; Stepanova et al. 2008; Rahman et al. 2010; Marquès-Bueno et al. 2021). As expected, we observed an impaired VGI response in the *wei8* mutant, a phenotype that was again (as in the case of ACC response) partially rescued by the excess auxin produced in the *sur2* background. Importantly, none of the high-order IAOx mutants showed significant deviation from the response observed in WT roots (Fig. 5B; Supplementary Data Set 1).

Another auxin-regulated process that is highly sensitive to alterations in IAA activity is the formation of lateral roots (Lavenus et al. 2013), with IAA controlling the initiation and emergence processes, as well as patterning (Marchant et al. 2002; Bao et al. 2014; Robbins and Dinneny 2018). Therefore, we next examined lateral root number in the high-order IAOx mutants. Quantification of the number of lateral roots in 10-d-old seedlings grown vertically under continuous light showed that *wei8* consistently produced fewer and *sur2* more lateral roots than WT, while the rest of the mutants had no appreciable alteration of this phenotype (Fig. 5C; Supplementary Data Set 1).

Finally, we examined the rapid hypocotyl elongation of seedlings grown in the light and exposed to high temperatures, as this is also a well-documented, auxin-dependent process (Ruegger et al. 1998). Hypocotyls of WT plants grown at 28 °C were approximately 4 times as long as those of seedlings grown at 21 °C (Fig. 5D; Supplementary Data Set 1). As expected, a defect in auxin biosynthesis like that of *wei8* translated into a significant reduction in the high-temperature-triggered hypocotyl elongation, a defect that was rescued by the increased auxin production in the *wei8 sur2* plants. In contrast, neither of the high-order IAOx mutants significantly altered the hypocotyl elongation response to high temperature in either the WT or the *sur2* mutant backgrounds.

In summary, none of the highly sensitive auxin-related phenotypic assays we carried out were able to detect significant phenotypic defects of the high-order *CYP71A*, *NIT*, and *AMI* family mutants. These results thus question the role of these gene families not only in the production of auxin under standard growth conditions, but also in response to abrupt changes in environmental or developmental factors (such as light regimen, temperature fluctuations, gravity vector changes in response to obstacle avoidance, or ethylene buildup in response to stress or soil compactness), as demonstrated here and elsewhere by utilizing classical phenotypic assays known to be highly sensitive to the levels of auxin (Stepanova et al. 2005, 2007) that allow us to visualize the mild auxin defects of the biosynthetic *wei8* mutant (Stepanova et al. 2008).

IAOx mutants do not show significant alterations in their IAOx/IAA metabolic profiles

In light of the lack of obvious morphological defects associated with auxin deficiency in the IAOx mutants after employing multiple highly sensitive assays, we decided to further explore the potential role of *CYP71A*, *NIT*, and *AMI* family genes in auxin biosynthesis by directly quantifying IAA; the IAA precursors anthranilate (ANT), TRP, IPyA, IAOx, IAN, and IAM; the inactivation products indole-3-acetyl-aspartate (IAA-Asp), indole-3-acetyl-glutamate (IAA-Glu), indole-3-acetyl-glucose (IAA-glc), and 2-oxindole-3-acetic acid (oxIAA); and the oxIAA-derived conjugated species (oxIAA-Asp, oxIAA-Glu, oxIAA-glc) (Fig. 1). To improve our ability to detect metabolic changes associated with altered IAA biosynthesis, we tested different growth conditions with the goal of identifying those conditions that would result in the strongest phenotypic differences between the WT, the weak auxin-deficient *wei8* mutant, and the *sur2* auxin overproducer. We found that when plants are grown in vertical plates for 3 d in the dark and then transferred to constant light for 4 additional days, *sur2* phenotypes such as small epinastic cotyledons and abundant adventitious roots were very prominent (Fig. 6). Interestingly, not only these *sur2* defects but also the *wei8* root gravity response and root meristem maintenance were strongly impaired under these growth conditions (Fig. 6) relative to plants grown in the same light regimen but in horizontal plates (Fig. 2; Supplementary Fig. S5). As expected, the excess auxin production in *sur2* partially rescued the root meristem size and root

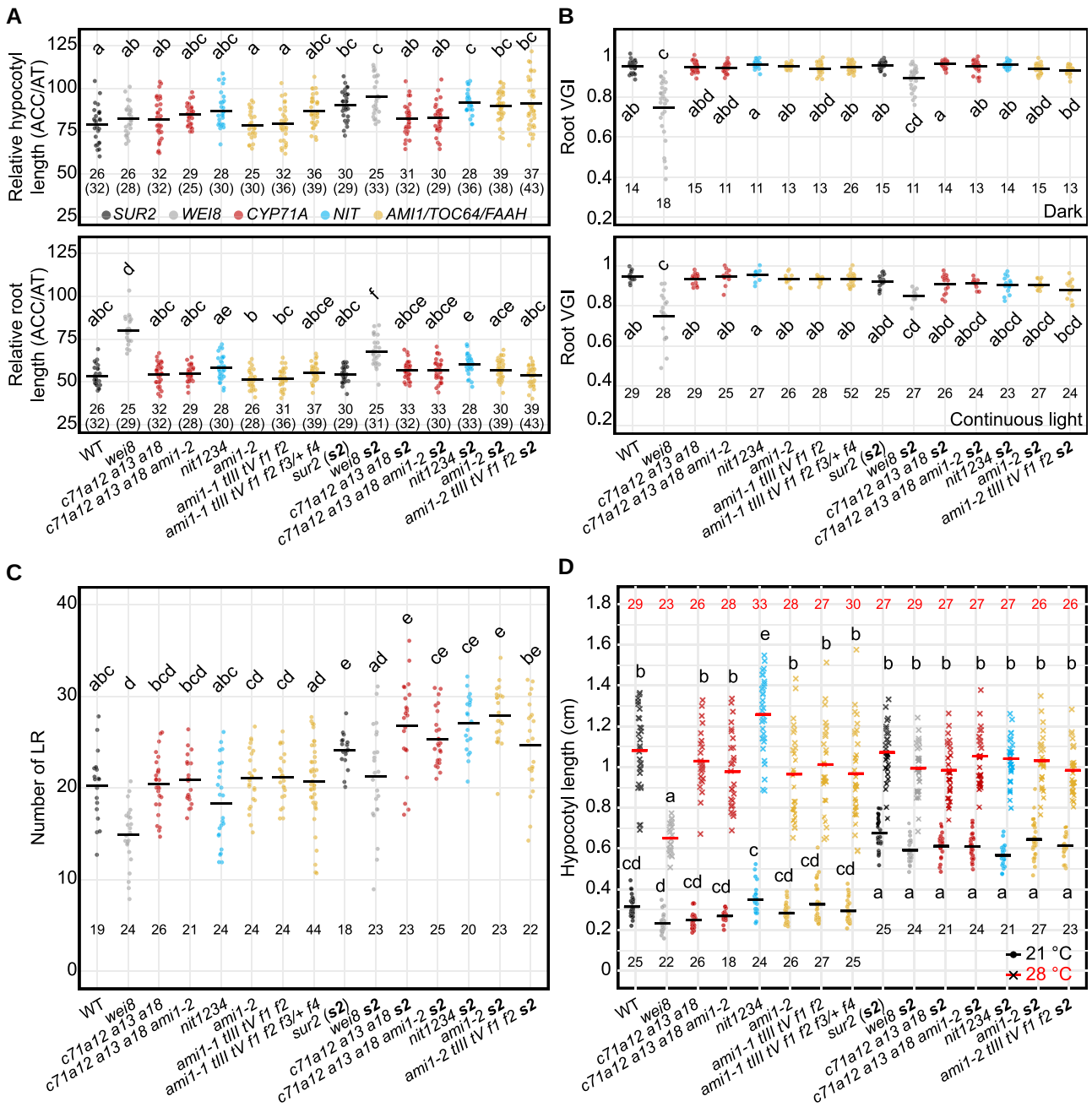

Figure 5. IAOx mutants do not show prominent phenotypes associated with auxin deficiency. **A)** Relative growth of hypocotyls (top) and roots (bottom) of 3-d-old, etiolated seedlings germinated on horizontal plates in the presence of the ethylene precursor ACC (0.2 µM). Relative length was calculated by dividing organ length in ACC by that in the control (AT). Statistical differences were analyzed using Kruskal–Wallis (1-way ANOVA on ranks) (hypocotyls) or ANOVA (roots) based on the criteria described in the methods section. **B)** Root vertical growth index (VGI, Grabov et al. 2005) of seedlings grown on vertical plates for 3 d in the dark (top) or for 5 d in the light (bottom). Statistical differences were analyzed using Kruskal–Wallis based on the criteria described in the methods section. **C)** Number of lateral roots in 10-d-old seedlings grown on vertical plates in continuous light. Statistical differences were analyzed using Poisson regression. **D)** Heat-induced hypocotyl elongation in 10-d-old, light-grown seedlings germinated on vertical plates. Statistical differences were analyzed using ANOVA of aligned rank transformed data (2-way ANOVA on ranks). Horizontal lines across datapoints represent mean values. Different letters denote statistically significant differences for $\alpha = 0.05$. Numbers below or above the datapoints represent the sample size for a given genotype and treatment. In panel A, numbers in brackets indicate the sample size used to calculate the mean value of a given genotype to normalize organ response to ACC. More details of statistical analyses results are available in Supplementary Data Set 1. Genotypes in WT or *sur2* background are color-coded by the mutated gene family: black (*SUR2*: WT and *sur2*), dark gray (*WEI8*: *wei8* and *wei8 sur2*), red (*CYP71A*: *c71a12a13a18*, *c71a12a13a18 ami1-2*, *c71a12a13a18 s2*, *c71a12a13a18 ami1-2 s2*), blue (*NIT*: *nit1234* and *nit1234 s2*), and yellow (*AMI1/TOC64/FAAH*: *ami1-2*, *ami1-1 tIII tV f1 f2*, *ami1-1 tIII tV f1 f2 f3/+ f4*, *ami1-2 s2*, *ami1-1 tIII tV f1 f2 s2*). WT: wild type (Col-0), *c71a12 a13 a18*: *cyp71a12 cyp71a13 cyp71a18*, *c71a12 a13 a18 ami1-2*: *cyp71a12 cyp71a13 cyp71a18 ami1-2*, *nit1234*: *nit1 nit2 nit3 nit4*, *ami1-1 tIII tV f1 f2*: *ami1-1 toc64-III toc64-V faah1 faah2*, *ami1-1 tIII tV f1 f2 f3/+ f4*: *ami1-1 toc64-III toc64-V faah1 faah2 faah3/+ faah4*, *s2*: *sur2*.

gravity defects of *wei8*. Even under these growth conditions, where the mild auxin biosynthetic defects of *wei8* were dramatically enhanced, the phenotypes of all of the high-order IAOx mutants were indistinguishable from those of the WT control plants. Nevertheless, we reasoned that these growth conditions were highly sensitive to alterations in the levels of auxin production

and, therefore, ideal for examining the ability of the IAOx high-order mutants to alter the IAA metabolic profile in the WT background or to block the expected alterations caused by the *sur2* mutation.

We next employed liquid chromatography coupled to tandem mass spectrometry (LC-MS/MS) to quantify the concentrations of IAA, its main biosynthesis precursors, and major storage and degradation products in WT; selected IAOx high-order mutants; and *wei8* in both WT and *sur2* mutant backgrounds (Fig. 7, Supplementary Fig. S13 and Supplementary Data Set 1). Due to the large difference in metabolite concentrations (for instance, IAA is only ~1% of total TRP; Supplementary Fig. S14A), to better visualize the data, we normalized each compound to its average WT concentration and represented the fold change by the relative size of the corresponding bubble (Fig. 7 and Supplementary Fig. S13). Consistent with previous reports (Novák et al. 2012), the concentration of IAOx dramatically increased in the *sur2* mutant. Not surprisingly, none of the high-order IAOx mutants had any effect on the high levels of IAOx accumulating in the *sur2* mutant (Fig. 7; Supplementary Data Set 1). Interestingly, an increase of between 60- and 120-fold in the levels of IAOx observed in all the lines in the *sur2* mutant background did not lead to a higher concentration of IAN or IAM (Fig. 7; Supplementary Data Set 1). Moreover, *sur2*-containing lines accumulated lower amounts of IAM than equivalent mutants without *sur2*, with the lowest IAM levels seen in the *ami1-2 toc64-III toc64-V faah1 faah2 sur2* mutant, which, based on the currently accepted models, would be expected to accumulate the highest concentration of this precursor by blocking the conversion of IAM into IAA.

In addition to higher IAOx concentrations in *sur2*-containing mutant lines, we observed a mild increase of auxin concentration, accompanied by a strong increase in the levels of IAA conjugation and oxidation products (Supplementary Fig. S13; Supplementary Data Set 1); metabolic changes were also reported previously for *sur2* (Novák et al. 2012; Pěnčík et al. 2013). These *sur2* metabolic changes were not affected by mutating any of the 3 IAOx gene families studied here. Finally, principal component analysis (PCA) of the IAA-related metabolic profiles showed that the main factor affecting the metabolic profiles in all our experiments is the *sur2* mutation, while none of the mutations in the IAOx gene families that were supposed to work downstream of *SUR2* in the production of IAA had any effect on the *sur2* metabolic profile (Supplementary Fig. S14B).

Together, these results are consistent with our genetic and pharmacological observations (Fig. 3; Supplementary Fig. S7) and strongly suggest that the previously proposed metabolic route for the production of IAA from IAOx via IAN and IAM, as well as the corresponding genetic pathway, needs to be thoroughly reevaluated.

Discussion

Several routes for the production of the key auxin IAA have been proposed (Fig. 1) (Zhao 2010). However, only the IPyA pathway has gathered enough experimental support to be generally accepted as the predominant source of IAA in all plants investigated (Zhao et al. 2001; Stepanova et al. 2008, 2011; Tao et al. 2008; Yamada et al. 2009; Zhou et al. 2011; Eklund et al. 2015). Two key factors hindered our ability to conclusively test the relevance of alternative IAA production routes. First, there was a lack of mutants that block the activity of entire multigene families coding for the enzymes thought to be involved in these metabolic pathways. Second, it is difficult to rule out possible biosynthetic pathways based on the absence of phenotypic defects in the corresponding knockout mutants, especially since these mutants can, inevitably, be examined only under a limited set of experimental conditions. To address these considerations, we took 3 complementary approaches. We began by generating high-order mutants knocking out all putative IAOx pathway genes in the 3 selected multigenic families that have been previously proposed to catalyze the conversion of IAN, IAM, or IAOx into IAA. We then examined the phenotypes of these whole-gene family knockouts under standard laboratory growth conditions as well as after specific treatments known to trigger phenotypic changes that are highly sensitive to auxin-level disturbances. We did this work not only in the WT but also in the *sur2* mutant background, where the IAOx pathways were believed to be hyperactive. Finally, in addition to this extensive phenotypic characterization, we also evaluated the metabolic profiles of the generated high-order mutants for a battery of IAA precursors and degradation products.

Our results conclusively show that the functions of the 3 gene families of *CYP71As*, *NITs*, and *AMIs* tested in this study are not required for the normal development of *Arabidopsis* plants under standard laboratory conditions. Importantly, the inability of these high-order mutants to block the high auxin phenotypes of *sur2* or to alter the characteristic metabolic profile of IAA-related compounds in the *sur2* mutant completely rules out any prominent role for these genes in the route of auxin production activated by the *sur2* mutation. These results not only disprove the previously proposed genetic pathway for the production of excess auxin in *sur2* (Fig. 1) but also cast doubts about the postulated metabolic pathway where the high levels of IAOx in *sur2* were thought to be converted into IAA via IAN and IAM. However, although we can discount the involvement of *CYP71A*, *NIT*, and *AMI* genes in the IAOx pathway and *sur2*-mediated auxin biosynthesis, we cannot rule out the involvement of the IAOx→IAN→IAM→IAA route itself in IAA production of excess auxin in *sur2*. It is still theoretically possible that these metabolic reactions are catalyzed by other, yet unknown enzymes. However, the possibility that this sequence of reactions is responsible for the high IAA levels operating in *sur2* is further weakened by our results from the treatment of the high-order mutants with the different auxin precursors, as summarized in Fig. 8. We showed that WT plants treated with each of the IAA precursors, IAOx, IAN, and IAM, displayed, as expected (Normanly et al. 1997; Buezo et al. 2019; Gao et al. 2020; Roman et al. 2023), auxin-related phenotypes (Fig. 4, Supplementary Fig. S8). Elimination of the *NIT* gene family function rendered clear resistance to IAN, indicating that nitrilase activities encoded by this gene family are required for the production of IAA from IAN taken up by the plant. Importantly, the *nit1/2/3/4* mutant showed normal response not only to IAA but also to IAOx. This was an unexpected result as, in the previously proposed metabolic pathway, IAN is an intermediate in the production of IAA from IAOx, and therefore, blocking the conversion of IAN into IAA should have also prevented the formation of IAA from IAOx via IAN. Furthermore, in disagreement with a mild insensitivity to IAM reported for the same *ami1-1* and *ami1-2* single mutants (Pérez-Alonso et al. 2021), our high-order *AMI* family mutant responded normally to all IAA precursors tested, including IAM, questioning the prominent role of AMI in the production of IAA in vivo. Conversely, the recently published *iamh1 iamh2* mutant showed clear resistance to IAM, as previously reported (Gao et al. 2020), firmly implicating the 2 *IAMH1 IAMH2* genes in the conversion of exogenous IAM to IAA in seedlings. The response to IAN and IAOx of the *iamh1 iamh2* mutant was, however, undisguisable from that of the WT plants in all growth conditions tested. These results, again, argue

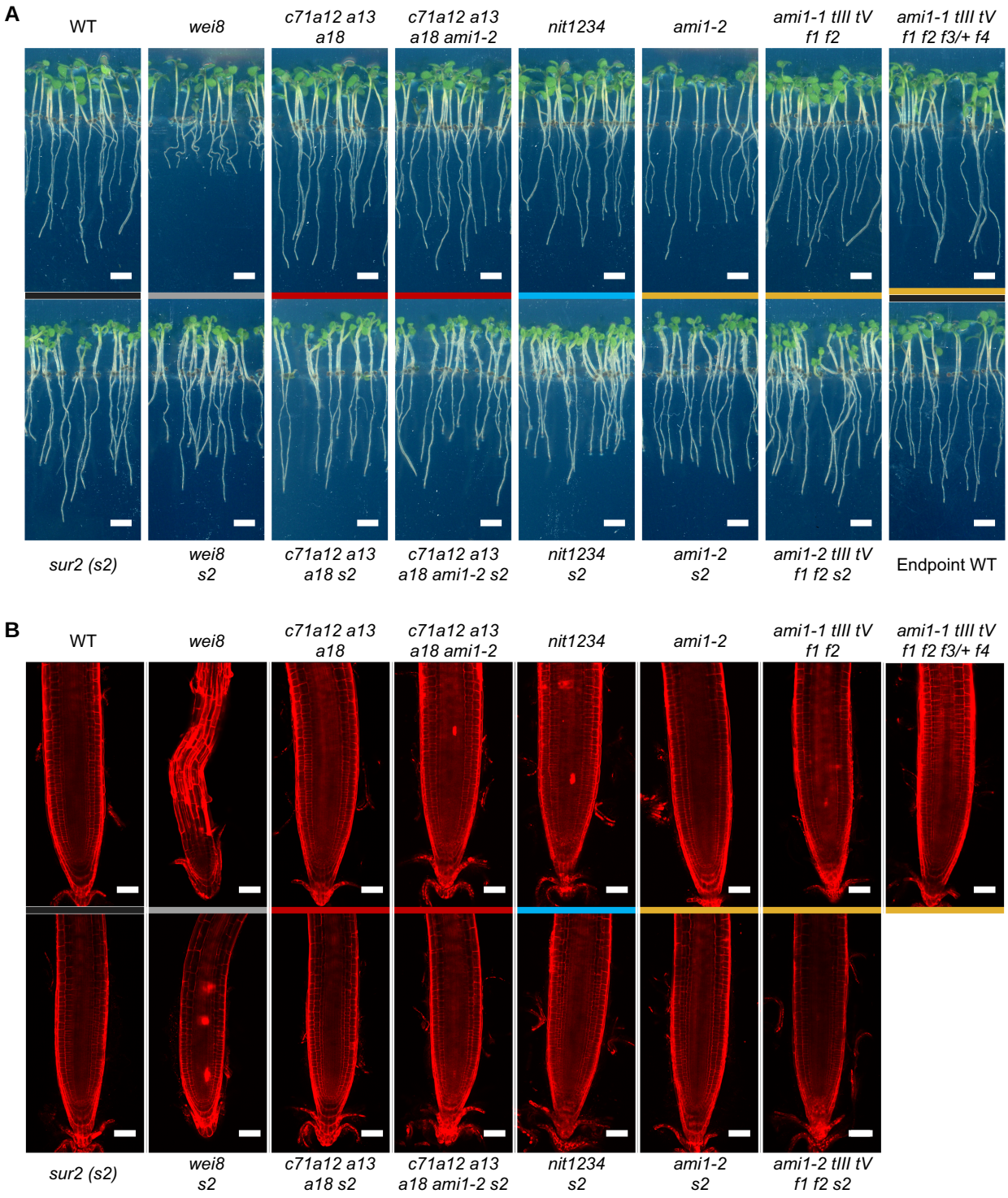

Figure 6. IAOx mutants grown on vertical plates do not show prominent phenotypes. **A)** The root growth defect of auxin-deficient *wei8* mutant is prominent when seedlings are grown on vertical plates for 3 d in the dark followed by 4 additional days in the light, whereas neither of the IAOx mutants displays prominent defects in these growth conditions. Scale bar = 1 cm. **B)** Propidium iodide-stained root tips of IAOx mutants are morphologically similar to that of WT plants, unlike that of *wei8* that show meristem degeneration. Scale bar = 50 µm. Genotypes in WT or *sur2* background are color-coded by the mutated gene family: black (*SUR2*: WT and *sur2*), dark gray (*WEI8*: *wei8* and *wei8 sur2*), red (*CYP71A*: *c71a12a13a18*, *c71a12a13a18 ami1-2*, *c71a12a13a18 s2*, *c71a12a13a18 ami1-2 s2*), blue (*NIT*: *nit1234* and *nit1234 s2*), and yellow (*AMI1/TOC64/FAAH*: *ami1-2*, *ami1-1 tIII tV f1 f2*, *ami1-1 tIII tV f1 f2 f3/+ f4*, *ami1-2 s2*, *ami1-1 tIII tV f1 f2 s2*). WT: wild type (Col-0), *c71a12 a13 a18*: *cyp71a12 cyp71a13 cyp71a18*, *c71a12 a13 a18 ami1-2*: *cyp71a12 cyp71a13 cyp71a18 ami1-2*, *nit1234*: *nit1 nit2 nit3 nit4*, *ami1-1 tIII tV f1 f2*: *ami1-1 toc64-III toc64-V faah1 faah2*, *ami1-1 tIII tV f1 f2 f3/+ f4*: *ami1-1 toc64-III toc64-V faah1 faah2 faah3/+ faah4*, *s2*: *sur2*.

against the previously proposed metabolic pathway model where both IAOx and IAN function as IAA precursors upstream of IAM. This is because if the model was accurate, blocking the conversion of IAM into IAA in the *iamh1 iamh2* mutant should result in resistance to both IAOx and IAN, which is not the case. Furthermore, our results indicate that neither of the 3 gene families investigated

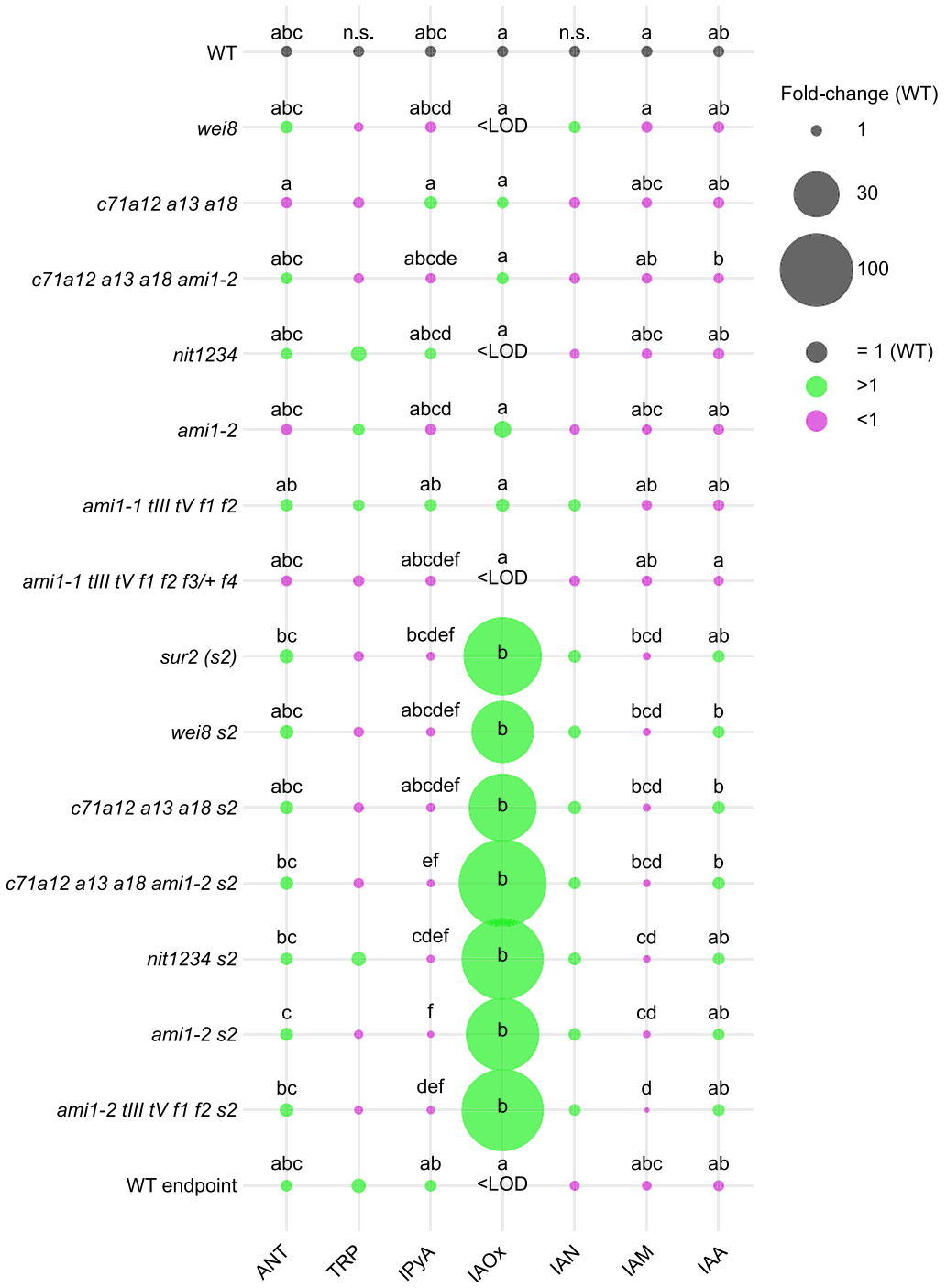

Figure 7. Metabolic quantification in IAOx mutants rules out a prominent role of *CYP71*, *NIT*, and *AMI1/TOC/FAAH* gene families in auxin biosynthesis. Concentrations are normalized to WT values for each metabolite. Bubble sizes are proportional to the concentration fold changes for each mutant compared to WT. Fold change of >1 is shown in green, and that of <1 is in magenta. Different letters denote statistically significant differences between mean values of metabolite concentrations (log10 (pmol g FW^{-1})) analyzed by ANOVA for $\alpha = 0.05$ ($n \geq 3$). More details of statistical analyses results are available in Supplementary Data Set 1. ANT: anthranilate, TRP: tryptophan, IPyA: indole-3-pyruvic acid, IAOx: indole-3-acetaldoxime, IAN: indole-3-acetonitrile, IAM: indole-3-acetamide, IAA: indole-3-acetic acid. WT: wild type (Col-0), *c71a12 a13 a18: cyp71a12 cyp71a13 cyp71a18*, *c71a12 a13 a18 ami1-2: cyp71a12 cyp71a13 cyp71a18 ami1-2*, *nit1234: nit1 nit2 nit3 nit4*, *ami1-1 tIII tV f1 f2: ami1-1 toc64-III toc64-V faah1 faah2*, *ami1-1 tIII tV f1 f2 f3/+ f4: ami1-1 toc64-III toc64-V faah1 faah2 faah3/+ faah4*, *s2: sur2*.

here, *CYP71As*, *NITs*, and *AMIs*, is involved in the excess auxin production in *sur2*.

One may argue that a possible reason for the lack of the *sur2* defect suppression by the mutants in the *CYP71A*, *NIT*, and *AMI* gene families characterized herein is that these putative IAOx pathway genes operate in different cell types from those where *SUR2* is expressed. In that scenario, other, yet unknown, enzymes would be responsible for the conversion of IAOx into auxin in *sur2*. However, there is at least a partial overlap in the cell types where *SUR2* and these other gene families are detected (Supplementary Fig. S15), so at least partial suppression of the *sur2* auxin defects would have been expected by the high-order IAOx family mutant

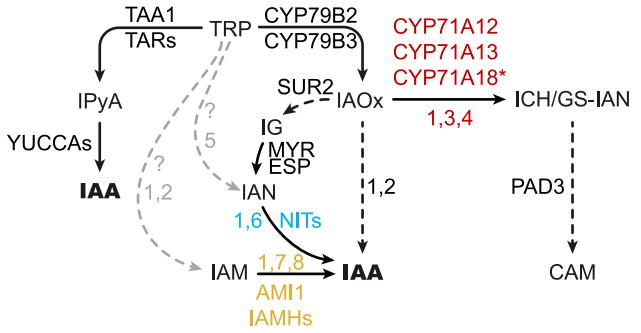

Figure 8. Revised model of tryptophan (TRP)-dependent auxin biosynthesis. Black and gray arrows represent high- and low-confidence enzymatic conversions, respectively. Solid arrows indicate single-step catalytic reactions, whereas dashed arrows represent multistep conversions. Numbers next to arrows correspond to references supporting the connections: (1) This work, (2) Sugawara et al. (2009), (3) Müller et al. (2015), (4) Mucha et al. (2019), (5) Zhao et al. (2002), (6) Normanly et al. (1997), (7) Pérez-Alonso et al. (2021), (8) Gao et al. (2020). IPyA: indole-3-pyruvic acid, IAA: indole-3-acetic acid, IAOx: indole-3-acetaldoxime, IAN: indole-3-acetonitrile, ICH: indole-3-cyanohydrin, GS-IAN: glutathione-indole-3-acetonitrile, IAM: indole-3-acetamide, IG: indole glucosinolate, CAM: camalexin; TAA1: TRP AMINOTRANSFERASE OF ARABIDOPSIS1 (WEI8), TAR: TAA1-RELATED (TAR1, TAR2), NITs: NITRILASE (NIT1–NIT4), IAMH: IAM HYDROLASE (IAMH1, IAMH2), MYR: MYROSINASE, ESP: EPITHIOSPECIFIER PROTEIN, PAD3: PHYTOALEXIN DEFICIENT3, ?: unknown enzyme(s). Note 1: *cyp71a12 cyp71a13* double mutant is CAM deficient (Müller et al. 2015) but not insensitive to IAOx; *cyp71a12 cyp71a13* is GS-IAN deprived (Müller et al. 2015) but not IAN deprived; and according to Mucha et al. (2019), CYP71A12 and CYP71A13 make indole-3-cyanohydrin. Since we did not quantify CAM-related compounds downstream of the CYP71 activity and due to the absence of phenotype in *cyp71a12 cyp71a13 cyp71a18* triple mutant generated in this work, the role of CYP71A18 in CAM biosynthesis is yet to be determined, hence showing a star (*). Note 2: *cyp79b2 cyp79b3* double mutant did not have detectable levels of IAN according to Sugawara et al. (2009), but according to Zhao et al. (2002), *cyp79b2 cyp79b3* did have detectable IAN. We found that the IAOx->IAN conversion is unlikely to be prominent in auxin biosynthesis, so IAN must have another source. The consensus in the field is that IGs are converted into IAN by means of myrosinases and epithiospecifier protein (Lambrix et al. 2001; Halkier and Gershenzon 2006). However, (Sugawara et al. 2009; Novák et al. 2012) reported that *sur2* and *sur1* (impaired in IG biosynthesis) have smaller but detectable amounts of IAN compared to WT, suggesting that IAN does not fully depend on IGs. Note 3: IAM is detected in the *cyp79b2 cyp79b3* mutant (Sugawara et al. 2009), suggesting that IAM production is not fully IAOx dependent. If auxin-like effects of exogenous IAOx or IAN depended on their conversion into IAM, *iamh1 iamh2* double mutant would be partially insensitive. Because *iamh1 iamh2* mutant is as sensitive to IAOx and IAN as WT, IAM may originate from another source.

combinations. One could also argue that the residual expression of *FAAH1* and *FAAH4*, as well as the remaining WT copy of *FAAH3*, in the high-order *ami1-1 toc64-III toc64-V faah1 faah2 faah3/+ faah4* mutant is the reason for the lack of auxin-deficient phenotypes in this mutant and for the inability of the *ami1-2 toc64-III toc64-V faah1 faah2* to suppress *sur2*. In a scenario where the spatiotemporal distribution of FAAH1, FAAH4, and FAAH3 proteins coincides with an overaccumulation of IAM as their low-affinity substrate (Pollmann et al. 2006), it could theoretically be possible that one or more of these FAAH members catalyze the IAM-to-IAA conversion. However, the low sequence identity that FAAH and AMI1 proteins share (Supplementary Fig. S1A) and the lack of prominent accumulation of IAM in our high-order mutants (Fig. 7), along with the reported very low in vitro activity of FAAH1 against IAM as a substrate, but strong activity against fatty acid amides (Shrestha et al. 2003, 2006; Pollmann et al. 2006; Kim et al. 2009; Khan et al. 2017), render this hypothetical scenario also unlikely.

Another intriguing observation we made in this work is the organ specificity of auxin activity resulting from growth media supplementation with IAOx, IAN, and IAM (Fig. 4 and Supplementary Fig. S8). The auxinic activity of these precursors has been previously described in independent studies under different growth conditions (Thimann and Mahadevan 1964; Normanly et al. 1997; Gao et al. 2020), but a systematic comparison of their spatial patterns of activity has not been reported. We found that the spatial patterns of *DR5* activity upon exogenous IAOx supplementation resemble those of IAA in all growth conditions tested (Fig. 4 and Supplementary Fig. S8), although much higher doses of IAOx are required to achieve comparable levels of growth inhibition. Discarding the possibility that IAOx is spontaneously converted to IAA in vitro (Supplementary Fig. S11), our results suggest that IAOx taken up by the root may be immediately converted into IAA, which would then follow the same transport patterns as those observed upon exogenous IAA supplementation, thus recapitulating IAA-induced *DR5* patterns of activity. In contrast to IAOx treatments, exogenous IAM supplementation did not translate into root shortening or increased *DR5* activity in roots. Instead, we observed high-auxin phenotypes in the aerial parts of the plant, such as hypocotyl elongation and epinastic leaves, suggesting that IAM is taken up from the medium by the root but is not directly converted into IAA in the root cells that have capacity to respond to and redistribute auxin within the root. Because we did not observe a strong induction of DR5 activity in roots, we argue that after being taken up from the media, IAM might be either immediately transported to aboveground tissues or first move radially to root vascular tissues to then be transported to the shoots. Upon reaching the root-hypocotyl junction, IAM may or may not be converted into IAA, and it remains to be studied whether it is distributed in the hypocotyl as IAM or as IAM-derived IAA.

The supplementation of media with IAN showed a mixed outcome, where all tissues showed changes in *DR5* activity and morphological responses to this precursor. Considering that IAN was thought to first be converted into IAM (Sugawara et al. 2009), and in our experiments a robust aboveground response is observed in IAM-supplemented seedlings, it was tempting to speculate that the aboveground response of IAN-supplemented plants may rely on the root transformation of IAN into IAM that is subsequentially transported to the shoot to be converted into IAA. However, in our study we report that *nit1/2/3/4* mutant is insensitive to IAN but sensitive to IAM, and *iamh1/2* shows normal sensitivity to IAN (Fig. 3 and Supplementary Fig. S7). If there was a significant nitrilase-independent conversion of IAN into IAM, we would expect *nit1/2/3/4* to show hypocotyl elongation similar to that observed upon IAM supplementation, and *iamh1/2* to be partially insensitive to IAN, which is not the case. Therefore, our results suggest that in our growth conditions, there is not a significant production of IAN-derived IAM in seedlings. Thus, the phenotype observed upon IAN supplementation must rely on a specific orchestration of IAN transport and conversion into IAA or another compound with auxinic activity.

In line with these hypotheses, the auxin import-deficient *aux1* mutant showed comparable insensitivity to IAOx and IAA, supporting the idea that IAOx is converted into IAA soon after it is taken up from the media (Fig. 3A). The hypocotyl response of *aux1* to IAM was impaired to a magnitude comparable to that observed in the IAM-insensitive *iamh1/2* mutant, suggesting that local

conversion of IAM into IAA alone cannot explain the phenotype observed, and that IAM-derived IAA import is required for hypocotyl elongation observed upon IAM supplementation (Fig. 3A). Finally, *aux1* root insensitivity to IAN was indistinguishable from that of the IAN-insensitive *nit1/2/3/4* mutant under low concentrations, but the *aux1* root insensitivity was far less prominent at higher IAN concentrations (Fig. 3A), implying the accumulation of IAN-derived IAA as a consequence of higher IAN amounts getting imported in an AUX1-independent manner, likely either through LAX transporters (Péret et al. 2012) or through diffusion.

From a biological perspective, it is also important to consider the functional significance of the aforementioned differences in auxin precursor activity patterns and the potential role these precursors play as molecular messengers for different types of environmental pressures. Specifically, IAOx is detected in silk-gland extract from the silkworm and regurgitant fluid from *Pontania* as a precursor of insect-produced IAA involved in gall formation (Suzuki et al. 2014; Yokoyama et al. 2017). IAN is a precursor of compounds involved in plant defense, such as CAM (Müller et al. 2015; Mucha et al. 2019), and a breakdown product of IG (Lambrix et al. 2001; Halkier and Gershenzon 2006), which may have an ecological relevance in modulating oviposition of *Pieris rapae* (de Vos et al. 2008) and preventing grazing from specialized herbivores (Lambrix et al. 2001). Finally, many plant-associated bacteria, including both plant growth-promoting rhizobacteria (PGPR) and phytopathogens, have been reported to produce IAA via IAM (Spaepen et al. 2007). Therefore, we speculate that the morphological changes in response to these metabolic precursors may play a functional role in plant defenses against insects and bacteria capable of producing these compounds.

Overall, our findings suggest that although exogenously provided IAOx, IAN, and IAM can indeed serve as precursors to IAA, the metabolic relationships previously proposed to link these compounds to the production of IAA in *sur2* should be reconsidered. The results from our targeted metabolic analysis are also inconsistent with what would be expected if the previously proposed metabolic and genetic pathways were correct. Thus, we did not observe any alteration in the endogenous levels of the examined metabolites, including IAA, IAA inactivation products, IAOx, IAN, and IAM, in our high-order mutants. It could be argued, however, that this is not strong evidence against the involvement of these gene families in the production of IAA under normal conditions, where the IAOx pathway may not be active. However, it would be more difficult to reconcile the lack of changes in the metabolic profiles of the IAA biosynthetic pathway when comparing *sur2*, where the IAOx pathway is supposed to be hyperactive, and our high-order IAOx mutants in the *sur2* mutant background.

Several key questions arise from the results presented in this study. How is excess IAA produced in the *sur2* mutant? Do the IAA production mechanisms activated in the *sur2* mutant play a physiological role in plants, and if so, are they necessarily restricted to *Brassicaceae* species? Finally, are *NIT*s and *IAMH*s involved in a yet uncharacterized IAA biosynthetic pathway? Even though we are currently unable to provide answers to these questions, this work has identified knowledge gaps that were previously ill-defined. Thus, for example, a hypothesis about how excess IAA is produced from extra IAOx in *sur2* needs to be formulated and tested. Toward that goal, our lab is currently carrying out genetic suppressor screens to identify mutant genes capable of masking the high-auxin phenotypes of *sur2*. Similarly, we have conducted a chemical screen to identify small molecules capable of suppressing the high *DR5:GUS* activity in the *sur2* mutant. Finally, we are performing a non-targeted metabolic analysis of *sur2* to identify compounds potentially involved in the conversion of IAOx into IAA in plants. Deciphering the mechanism by which excess auxin is produced in *sur2* would open the door to investigating whether these mechanisms are also active in WT plants under specific conditions or in response to certain biotic or abiotic factors. One may argue that since IAOx and the corresponding biosynthetic enzymes CYP79B2 and CYP79B3 have not been found outside the *Brassicaceae* family, any potential physiological relevance of this pathway found in *Arabidopsis* would be restricted to a small group of plants. However, the discovery of PAOxs and their corresponding biosynthetic enzymes in both monocot and dicot leaves (Perez et al. 2021), along with the observation that IAOx triggers auxin signaling and *sur2*-like phenotypes in a *Fabaceae* species, *M. truncatula* (Buezo et al. 2019; Roman et al. 2023), and can be converted to IAA in other non-*Brassicaceae* species (Rajagopal and Larsen 1972), opens the possibility that insights gained about the IAOx pathways in *Arabidopsis* could have implications beyond *Brassicaceae* family.

Materials and methods

Generation of mutant lines

T-DNA lines and their respective insertion sites are depicted in Supplementary Fig. S2. Higher-order mutant combinations were obtained by crossing, and the desired mutant combinations were identified by genotyping. All the mutant lines generated in this work and their sources are listed in Supplementary Table S1. Primer sequences and primer combinations used for genotyping are available in Supplementary Tables S2 and S3, respectively. *CYP71A* triple KO mutant (*cyp71a12/a13/a18*) was obtained by crossing the previously described *cyp71a12*^{TALENs}*/a13* double mutant (Müller et al. 2015) to *cyp71a18* available from Arabidopsis Biological Resource Center (ABRC). *nit3* and *nit4* mutants were also ordered from ABRC and intercrossed. Due to the tight linkage between *NIT1*, *NIT2*, and *NIT3*, CRISPR/Cas9 genome editing was employed to obtain higher-order *nit* mutants. The guide RNA (gRNA) (5′-ATTGGAAAACTCGGTGCTGC-3′) was cloned into pDONR207 by site-directed, ligase-Independent mutagenesis (SLIM) (Chiu 2004) using the following primers: SLIM_F GTTTTAGAGCTAGAAATAGCAAG, SLIM_R CAATCACTACTTCGACTCT, NITDFor_tailed GCAGCACCGAGTTTTCCAATGTTTTAGAGCTAGAAATAGCAAG, and NITDRev_tailed ATTGGAAAACTCGGTGCTGCCAATCACTACTTCGACTCT. Briefly, 2 separate inverse PCR amplifications (SLIM_F + NITDRev_tailed and NITDFor_tailed + SLIM_R) were pooled, treated with *DpnI*, melted, reannealed to obtain a linear vector with 20-mer sticky ends, and directly transformed into *Escherichia coli* (*E. coli*). The pDONR207_gRNA plasmid was extracted using alkaline lysis and the gRNA was moved into the Gateway-compatible binary vector pMTN3164 (Denbow et al. 2017) by LR reaction using manufacturer-recommended protocols (Thermo Fisher Scientific). gRNA integrity was confirmed by Sanger sequencing using primers CAS9zn_GW_For TACAACAGTCTTGACACAGTCTCCC and CAS9zn_GW_Rev AGATAGCCCAGTAGCTGACATTCAT.

Arabidopsis nit3 nit4 double-mutant plants were grown in soil under long-day photoperiod, 16-h light/8-h dark, at 20 °C. Transformation was carried out using the floral dip method (Clough and Bent 1998), using *Agrobacterium tumefaciens C58* harboring the gRNA in pMTN3164. T1 transformants were selected on half-strength Murashige and Skoog medium supplemented with 20 μg/mL hygromycin under the described growth

conditions. After 2 wk, transformed seedlings with true leaves and roots were transferred to soil. A single rosette leaf per T1 plant was harvested, its genomic DNA extracted, and genotyping PCRs performed to confirm the presence of *Cas9* (using internal primers CAS9 inter For: TCCACTGGCTAGAGGCAACT, and CAS9 inter Rev: GCGATATGCTCGTGAAGTGA) and somatic CRISPR-induced deletions in the *NIT2-NIT1* region (Supplementary Tables S2 and S3). The size of the PCR product of the WT *NIT2-NIT1* region was 4.4 kb, whereas the size of the PCR product of the deleted region was 0.8 kb. Similarly, T2 plants were genotyped to identify plants without the *Cas9* construct but that harbored the *NIT2-NIT1* deletion. In T3 plants, the homozygosity of the deleted region was confirmed by PCR. Sequencing of the deleted region was performed to rule out the possibility of the generation of a potential chimeric protein resulting from the fusion of the 5′ end of *NIT2* and the 3′ end of *NIT1* genomic regions. The sequencing revealed an insertion of an additional G (Supplementary Fig. S3) that produced a frameshift leading to a premature stop codon 10 amino acids downstream of the targeted site. The selected *Cas9*-free homozygous *nit1 nit2 nit3 nit4* plants were then crossed to *nit3 nit4 sur2* plants to obtain the final *nit1 nit2 nit3 nit4 sur2* quintuple mutant.

AMI1 gene mutants, *ami1-1* (SALK_069970) and *ami1-2* (SALK_019823), were obtained from ABRC. Mutants in the *TOC64* and *FAAH* family members were obtained from other laboratories: *ami1-1 toc64-III-1 toc64-V-1* (Aronsson et al. 2007) was a gift from Paul Jarvis (Oxford University) and Henrik Aronsson (University of Gothenburg), and *faah1 faah2* (Keereetaweep et al. 2013) was provided by Kent Chapman (University of Northern Texas) and Elison Blancaflor (Noble Foundation). *aux1-7* (Pickett et al. 1990), *wei8-1* (Stepanova et al. 2008), *sur2* (Delarue et al. 1998; Stepanova et al. 2005), *cyp79b2 b3* (Zhao et al. 2002), and *cyp79b2 b3 s2* (Stepanova et al. 2011) mutants, as well as *YUCCA1* overexpression line (*YUCox*) (Zhao et al. 2001), have been previously described. The *iamh1-1 iamh2-2* (Gao et al. 2020) mutant was a gift from Prof. Hiroyuki Kasahara (Tokyo University of Agriculture and Technology).

Growth conditions

Seeds were surface-sterilized using a solution consisting of 50% commercial bleach supplemented with 0.01% Triton X-100 for 5 min, washed with sterile de-ionized water 4 times, and stratified for 3 d at 4 °C prior to starting any assay. For ACC sensitivity assay, seeds were resuspended in sterile 0.6% low-melting-point (LMP) agarose, sowed in aseptic conditions on the surface of sterile AT media (4.33 g/L Murashige and Skoog salts, 10 g/L sucrose, pH 6.0 adjusted with 1 M KOH, 6 g/L Bacto Agar) and AT supplemented with 0.2 µM ACC. Germination was induced under ambient light for 2 h at room temperature and the plates were transferred to the dark at 22 °C and kept horizontally. After 72 h, seedlings were individually transferred onto another plate for imaging. For quantification of seedling sensitivity to IAA (Sigma-Aldrich) and IAA precursors IAOx (Ambeed), IAN (Sigma-Aldrich), IAM (Sigma-Aldrich), seed sowing and germination on supplemented plates were identical to those described for ACC, with the assays run in horizontal plates under a range of precursor concentrations, as shown in Supplementary Table S4, either under continuous LED light (70–100 µmol m^{-2} s^{-1}; 2× 6000 K Kihung T8 LED integrated fixture 40W + 1× FULL SPECTRUM Monios-L LED grow light full spectrum 60W) for 5 d or in the dark for 3 d.

For *DR5:GFP* reporter activity assays, seed sowing and germination on supplemented plates were identical to those described for the IAA precursor treatments, selecting the concentrations of IAA intermediates that produce comparable degree of phenotypic responses across all precursor treatments. For plant imaging, seedlings germinated on supplemented plates were transferred to plain 0.8% (w/v) Bacto Agar plates and imaged using Leica Thunder Imager M205FA equipped with Leica DMC6200 color camera (bright field) and Leica DFC9000 sCMOS camera (fluorescence). For shorter 16-hour precursor treatments, seedlings were sowed and germinated on horizontal plates, as described for ACC assays, but on control (AT) plates without ACC supplementation. Dark-germinated seedlings were grown for ∼2.5 d, transferred onto supplemented plates, and grown vertically for additional 16 h in the dark before imaging to complete 72 h. Light-germinated seedlings were grown for ∼4.5 d, transferred onto supplemented plates, and grown vertically for additional 16 h under continuous LED light before imaging.

To assess VGI (Grabov et al. 2005), seed sowing and germination on supplemented plates were identical to those described for ACC. Seeds were resuspended in 0.2% (w/v) LMP agarose, and sowed on square AT plates for vertical growth (10 g/L Bacto Agar) in a line containing 20–30 seeds. Germination was induced as described above and plates were placed vertically at 22 °C in the dark or under continuous LED light for 5 d prior to image acquisition. For the quantification of lateral roots, seeds were sowed and germinated as described for VGI and grown vertically under continuous light for 10 d prior to imaging. Counting of emerged lateral roots was assisted by a Nikon SMZ645 stereo microscope, and small bulges without epidermal opening were not counted. For heat-induced hypocotyl elongation tests, seed sowing and germination were identical to those described for the VGI experiment, and assays were performed as described (Zhu et al. 2021) in Percival I-36LL chambers with INTELLUS control system under constant fluorescent light (70 µmol m^{-2} s^{-1}). For metabolic profiling, seeds were surface-sterilized, sowed and germinated as described for VGI, and grown in the dark for 3 d followed by 4 d under continuous LED light. Seven-day-old seedlings were harvested and flash-frozen in liquid nitrogen, ground manually using a liquid nitrogen-prechilled mortar and pestle, and weighed prior to sample lyophilization.

To image adult plants grown in soil, seeds were sowed and germinated as described for the VGI assay. Plates were then placed vertically in the dark for 3 d at 22 °C and transferred to continuous light for 4 more days prior to imaging. Then, seedlings were transferred to soil (1:1 ratio of SunGro professional growing mix and Jolly Gardener Pro-Line C/B growing mix) to standard 4×6 flats (Greenhouse Megastore), at 5 seedlings per each pot, 4 pots per genotype. Pot positions were semi-randomized, with the pots periodically reshuffled to minimize positional effects. Plants were grown for 2 more weeks under white light using fluorescent bulbs (EIKO F54T5/HO/850 TCLP 1C2) in long-day conditions (16-h light/8-h dark) at 22 °C prior to imaging using an OLYMPUS PEN Lite E-PL6 camera.

Quantification of auxin, auxin precursors, and auxin metabolites

Auxin metabolite profiles were analyzed using liquid chromatography–tandem mass spectrometry (LC-MS/MS) following the method described by (Novák et al. 2012). Briefly, approximately 10 mg of fresh weight per sample were lyophilized and extracted with 1 mL of cold 50 mM phosphate buffer (pH 7.0) containing 0.1% sodium diethyldithiocarbamate and a mixture of stable isotope-labelled internal standards. First, 500 µL portion of the centrifuged extract was acidified to pH 2.7 with HCl and purified

by solid-phase extraction (SPE) using Oasis™ HLB columns (30 mg, 1 mL; Waters, USA). Second, 500 µL portion was derivatized with cysteamine, acidified to pH 2.7 with HCl, and purified by SPE to determine IPyA. Following elution, all samples were evaporated under reduced pressure, reconstituted in 10% aqueous methanol, and analyzed using I-Class UHPLC system (Waters, Milford, CT, USA) equipped with Kinetex C18 column (50 mm × 2.1 mm, 1.7 µm; Phenomenex) and coupled to a triple quadrupole mass detector (Xevo TQ-S; Waters, USA).

Assessment of spontaneous conversion of IAOx into IAA

Chemical standards of IAA and IAOx were analyzed on an Agilent G6530A QTOF LC/MS instrument. A Zorbax Eclipse Plus C18 column (3 × 100 mm, 1.8 µm) was used with a binary gradient of 0.1% (v/v) formic acid in water (solvent A) and 0.1% (v/v) formic acid in acetonitrile (solvent B) at a flow rate of 0.6 mL min^{-1}. The gradient started at 5% solvent B for 1 min, followed by a linear increase to 65% B over 6 min, then to 95% B over 1 min, and held at 95% B for 2 min. The acquisition of mass spectra was done in the positive ionization mode with the following parameters: drying gas temperature, 300 °C; drying gas flow rate, 7.0 L min^{-1}; nebulizer pressure, 40 psi; sheath gas temperature, 350 °C; sheath gas flow rate, 10.0 L min−1; Vcap, 3500 V; Nozzle Voltage, 500 V; Fragmentor, 150 V; Skimmer, 65.0 V; Octopole RF Peak, 750 V.

RNA extraction and qPCR

Seeds from each genotype were sown on 8 g/L agar plates and incubated horizontally under continuous light at 22 °C for 10 d prior to tissue collection. Seedlings from 2 plates per genotype were harvested and flash frozen in liquid nitrogen. Frozen seedlings were ground in a liquid nitrogen-prechilled mortar, and 100 mg of pulverized tissue from each genotype were mixed with 1 mL of Trizol LS reagent (Invitrogen) per sample and phase separated using chloroform. RNA was extracted from the upper aqueous phase using the Qiagen RNeasy Kit following the manufacturer protocol (Qiagen) with an on-column DNase treatment for 15 min at 30 °C (Qiagen). First-strand cDNA synthesis was performed on 100 ng of total RNA using an oligo-d(T)18 primer and 2 µL of SuperScriptIII reverse transcriptase (Invitrogen). Reverse transcription reactions were incubated for 1 h at 50 °C, 15 min at 55 °C, followed by 15 min at 70 °C for enzyme deactivation. The product of each reaction was diluted 5-fold and 3 µL of the dilution were used as a template for RT-qPCR with a SYBR Green PCR Mastermix (Applied Biosystems) in a StepOnePlus Real-Time PCR system (Applied Biosystems). A default program of 10 min at 95 °C, followed by 40 cycles of {15 s at 95 °C, 30 s at 60 °C} was utilized.

To compare levels of expression across different genotypes, primers were designed to amplify a < 250 bp region at the 3′ end of mature transcripts. For all gene targets, one or both primer sequences overlapped an exon-exon junction to selectively amplify from cDNA. Primer efficiency was determined for each primer pair using a serial dilution of WT (Col-0) cDNA, with 3 replicates per sample. Given similar primer efficiencies, relative gene expression was evaluated using the $\Delta\Delta C_T$ method (Livak and Schmittgen 2001) . For all targets, RT-qPCR was performed using 3 biological replicates per genotype. Primers used in expression analysis of intronic alleles by qPCR are available in Supplementary Table S5, and annealing sites are depicted in Supplementary Fig. S2.

Image acquisition and statistical analysis

For the analysis of seedling morphometric traits (ACC-mediated hypocotyl and root shortening, VGI, heat-induced hypocotyl elongation, and counting of emerged lateral roots), seedling images were acquired using an Epson Perfection V600 Photo scanner and analyzed with FIJI/ImageJ. Data plotting and statistical analysis were performed using R studio pipelines utilizing car (Fox and Weisberg 2019), pwr (Champely 2020), rstatix (Kassambara 2023), dunn.test (Dinno 2024), and multcompView (Graves et al. 2024) packages. First, we removed outliers, defined based on Tuckey's criteria: $x < Q1 - 1.5 \times IQR$ and $x > Q3 + 1.5 \times IQR$, with IQR (interquartile range) = Q3−Q1. Next, we tested whether the dataset fitted a normal distribution (Shapiro-Wilk test; Shapiro and Wilk 1965) and presented homoscedasticity (Levene test; Levene 1960) prior to running the hypothesis contrast analyses. If a dataset was homoscedastic and it had strong statistical power (power = $1 - \beta >$ 0.8, with β being the probability of accepting the null hypothesis when it is actually false), we performed ANOVA followed by post-hoc Tukey test regardless of whether it was normally distributed ($\alpha = 0.05$). Otherwise, the dataset was transformed using log10 and retested for homoscedasticity and power. If after data transformation the abovementioned requirements for ANOVA/Tukey were not met, we performed non-parametric Kruskal-Wallis test (Kruskal and Wallis 1952), followed by Dunn's test (Dunn 1961, 1964) for $\alpha = 0.05$. In the case of lateral root formation (Fig. 5C), data distribution follows a Poisson distribution, and it is thus not suitable for ANOVA. Instead, statistical differences were tested using Poisson Regression (McCullagh and Nelder 1989; Cameron and Trivedi 1998).

Accession numbers

AT1G70560 (*WEI8/TAA1*), AT4G31500 (*SUR2*), AT2G30750 (*CYP71A12*), AT2G30770 (*CYP71A13*), AT1G11610 (*CYP71A18*), AT3G44310 (*NIT1*), AT3G44300 (*NIT2*), AT3G44320 (*NIT3*), AT5G22300 (*NIT4*), AT1G08980 (*AMI1*), AT3G17970 (*TOC64-III*), AT5G09420 (*TOC64-V*), AT5G64440 (*FAAH1*), AT5G07360 (*FAAH2*), AT3G25660 (*FAAH3*), AT4G34880 (*FAAH4*), AT2G38120 (*AUX1*), AT4G39950 (*CYP79B2*), AT2G22330 (*CYP79B3*), AT4G37550 (*IAMH1*), AT4G37560 (*IAMH2*).

Acknowledgments

We are grateful to Drs. Paul Jarvis (Oxford University), Henrik Aronsson (University of Gothenburg), Kent Chapman (University of Northern Texas), Elison Blancaflor (Noble Foundation), and Hiroyuki Kasahara (RIKEN Center for Sustainable Resource Center, Japan) for kindly sharing mutant seeds with us. We also thank Dr. Jose Bruno-Barcena (NC State University, USA) for his assistance with plant sample lyophilization, Drs. Miguel Flores Vergara and Robert Franks for sharing reagents and equipment, and members of the Alonso-Stepanova laboratory and the INTRINSyC community at NCSU for their valuable feedback and discussions.

Author contributions

A.N.S. and J.M.A. conceived the project. A.N.S., J.M.A., and M.F. designed the research. A.N.S., J.B., and M.F. generated *Arabidopsis* mutants. A.Pě. performed the quantitative profiling of auxin-related metabolites. B.E. performed quantitative analysis of gene expression of intronic T-DNA alleles. J.D. and A.Pa. contributed to the identification of high-order mutants. X.L. tested the spontaneous conversion of IAOx into IAA in vitro. M.F. conducted

experiments, analyzed the data, and prepared figures. S.B. contributed to the analysis of the results. A.N.S., J.M.A., K.L., O.N., and M.M.K. supervised research. M.F., A.N.S., and J.M.A. wrote the manuscript with the contributions of other authors.

Supplementary data

The following materials are available in the online version of this article.

Supplementary Figure S1. Phylogenetic comparison of the amino acid sequences of *Arabidopsis* CYP71A, NIT, and AMI1/TOC64/FAAH family members.

Supplementary Figure S2. Schematic representation of the gene structure (5′ to 3′) of *CYP71A*, *NIT*, and *AMI1/TOC64/FAAH* gene families examined in this study.

Supplementary Figure S3. Genome editing of tandem *NITRILASE2* (*NIT2*) and *NIT1* genes.

Supplementary Figure S4. Embryo lethality in 2 independent *faah3* mutant alleles observed in dissected siliques.

Supplementary Figure S5. Mutants defective in the proposed IAOx pathway of auxin biosynthesis do not display obvious growth defects.

Supplementary Figure S6. Expression analysis of intronic T-DNA alleles shows that *AMI1* is inactivated, but *FAAH1* and *FAAH4* are only partially knocked down.

Supplementary Figure S7. Phenotypes of dark-grown mutants impaired in the putative IAOx route challenge the established model of the IAOx pathway.

Supplementary Figure S8. Exogenous application of putative IAOx intermediates induces the auxin response reporter *DR5:GFP*.

Supplementary Figure S9. IAOx pathway mutants show normal root sensitivity to IAA.

Supplementary Figure S10. *iamh1 iamh2 sur2* mutants are indistinguishable from *sur2*.

Supplementary Figure S11. The IAOx stock is not spontaneously converted into IAA.

Supplementary Figure S12. IAOx pathway mutant hypocotyls and roots show WT-like responses to exogenous ACC.

Supplementary Figure S13. Metabolic quantification of IAA and its degradation products in IAOx shows major upregulation of homeostasis mechanisms leading to higher auxin degradation in *sur2*.

Supplementary Figure S14. *sur2* is the only tested mutation that prominently impacts the metabolic profiles of *Arabidopsis* seedlings.

Supplementary Figure S15. Single-cell gene expression analysis shows an overlap in the cortex cells, but not in the quiescent center (QC), among the gene families studied in this work.

Supplementary Table S1. Mutant lines used or generated in this work and their stock numbers.

Supplementary Table S2. Primer combinations used for genotyping and PCR product size.

Supplementary Table S3. Primer sequences used for mutant genotyping.

Supplementary Table S4. Concentrations (μM) of auxin biosynthesis precursors used in assays shown in Fig. 3A and Supplementary Fig. S6B.

Supplementary Table S5. Primer combinations used for expression analysis of intronic T-DNA alleles by RT-qPCR.

Supplementary File 1. CYP71A13.fasta.

Supplementary File 2. NIT1.fasta.

Supplementary File 3. AMI1.fasta.

Supplementary File 4. CYP71A13.nwk.

Supplementary File 5. NIT1.nwk.

Supplementary File 6. AMI1.nwk.

Funding

This work was supported by the National Science Foundation (NSF) grants 0923727, 1444561, and 2327912 to J.M.A. and A.N.S.; 1158181 and 0519869 to J.M.A.; and 1750006 to A.N.S., and leveraged microscopy equipment available at the NCSU's Cellular and Molecular Imaging Facility (NSF grant 1624613). S.B. was supported by EVOFRULAND H20MC_RISE21LCOLO_02 CUP G45F21002810006. K.L. acknowledges grants from the Knut and Alice Wallenberg Foundation (KAW 2016.0352, KAW 2020.0240) and the Swedish Research Council (VR 2021-04938).

Conflict of interest statement. The authors declare that they have no competing interests to disclose.

Data availability

The data corresponding to this article are available within the article itself or in its online supplementary materials.

References

Aronsson H, Boij P, Patel R, Wardle A, Töpel M, Jarvis P. Toc64/OEP64 is not essential for the efficient import of proteins into chloroplasts in *Arabidopsis thaliana*. *Plant J*. 2007:52(1):53–68. https://doi.org/10.1111/j.1365-313X.2007.03207.x

Bak S, Nielsen HL, Halkier BA. The presence of CYP79 homologues in glucosinolate-producing plants shows evolutionary conservation of the enzymes in the conversion of amino acid to aldoxime in the biosynthesis of cyanogenic glucosides and glucosinolates. *Plant Mol Biol*. 1998:38(5):725–734. https://doi.org/10.1023/A:1006064202774

Bak S, Tax FE, Feldmann KA, Galbraith DW, Feyereisen R. CYP83B1, a cytochrome P450 at the metabolic branch point in auxin and indole glucosinolate biosynthesis in *Arabidopsis*. *Plant Cell*. 2001:13(1):101–111. https://doi.org/10.1105/tpc.13.1.101

Bao Y, Aggarwal P, Robbins NE, Sturrock CJ, Thompson MC, Tan HQ, Tham C, Duan L, Rodriguez PL, Vernoux T, et al. Plant roots use a patterning mechanism to position lateral root branches toward available water. *Proc Natl Acad Sci U S A*. 2014:111(25):9319–9324. https://doi.org/10.1073/pnas.1400966111

Barlier I, Kowalczyk M, Marchant A, Ljung K, Bhalerao R, Bennett M, Sandberg G, Bellini C. The *SUR2* gene of *Arabidopsis thaliana* encodes the cytochrome P450 CYP83B1, a modulator of auxin homeostasis. *Proc Natl Acad Sci U S A*. 2000:97(26):14819–14824. https://doi.org/10.1073/pnas.260502697

Bennett MJ, Marchant A, Green HG, May ST, Ward SP, Millner PA, Walker AR, Schulz B, Feldmann KA. *Arabidopsis* AUX1 gene: a permease-like regulator of root gravitropism. *Science*. 1996:273(5277):948–950. https://doi.org/10.1126/science.273.5277.948

Boerjan W, Cervera MT, Delarue M, Beeckman T, Dewitte W, Bellini C, Caboche M, Van Onckelen H, Van Montagu M, Inzé D. Superroot, a recessive mutation in *Arabidopsis*, confers auxin overproduction. *Plant Cell*. 1995:7(9):1405–1419. https://doi.org/10.1105/tpc.7.9.1405

Brumos J, Robles LM, Yun J, Vu TC, Jackson S, Alonso JM, Stepanova AN. Local auxin biosynthesis is a key regulator of plant development. *Dev Cell*. 2018:47(3):306–318.e5. https://doi.org/10.1016/j.devcel.2018.09.022

Buezo J, Esteban R, Cornejo A, López-Gómez P, Marino D, Chamizo-Ampudia A, Gil MJ, Martínez-Merino V, Moran JF. IAOx induces the SUR phenotype and differential signalling from IAA under different types of nitrogen nutrition in *Medicago truncatula* roots. *Plant Sci*. 2019:287:110176. https://doi.org/10.1016/j.plantsci.2019.110176

Cameron AC, Trivedi PK. *Regression analysis of count data*. 2nd ed. Cambridge (England): Cambridge University Press; 1998.

Champely S. *PWR: basic functions for power analysis*. R Package Version. 1; 2020.

Chiu J. Site-directed, Ligase-Independent Mutagenesis (SLIM): a single-tube methodology approaching 100% efficiency in 4 h. *Nucleic Acids Res*. 2004:32(21):e174–e174. https://doi.org/10.1093/nar/gnh172

Clough SJ, Bent AF. Floral dip: a simplified method for *Agrobacterium*-mediated transformation of *Arabidopsis thaliana*. *Plant J*. 1998:16(6):735–743. https://doi.org/10.1046/j.1365-313x.1998.00343.x

Cooney TP, Nonhebel HM. Biosynthesis of indole-3-acetic acid in tomato shoots: measurement, mass-spectral identification and incorporation of 2 H from 2 H 2 O into indole-3-acetic acid, D- and L-tryptophan, indole-3-pyruvate and tryptamine. *Planta*. 1991:184(3):368–376. https://doi.org/10.1007/BF00195339

Delarue M, Prinsen E, Onckelen VH, Caboche M, Bellini C. *Sur2* mutations of *Arabidopsis thaliana* define a new locus involved in the control of auxin homeostasis. *Plant J*. 1998:14(5):603–611. https://doi.org/10.1046/j.1365-313X.1998.00163.x

Denbow CJ, Lapins S, Dietz N, Scherer R, Nimchuk ZL, Okumoto S. Gateway-compatible CRISPR-Cas9 vectors and a rapid detection by high-resolution melting curve analysis. *Front Plant Sci*. 2017:8. https://doi.org/10.3389/fpls.2017.01171

de Vos M, Kriksunov KL, Jander G. Indole-3-acetonitrile production from indole glucosinolates deters oviposition by *Pieris rapae*. *Plant Physiol*. 2008:146(3):916–926. https://doi.org/10.1104/pp.107.112185

Dinno A. *dunn.test: Dunn's test of multiple comparisons using rank sums*. R package version 1.3.6; 2024. *https://CRAN.R-project.org/package=dunn.test*

Dunn OJ. Multiple comparisons among means. *J Am Stat Assoc*. 1961:56(293):52–64. https://doi.org/10.1080/01621459.1961.10482090

Dunn OJ. Multiple comparisons using rank sums. *Technometrics*. 1964:6(3):241–252. https://doi.org/10.1080/00401706.1964.10490181

Eklund DM, Ishizaki K, Flores-Sandoval E, Kikuchi S, Takebayashi Y, Tsukamoto S, Hirakawa Y, Nonomura M, Kato H, Kouno M, et al. Auxin produced by the indole-3-pyruvic acid pathway regulates development and gemmae dormancy in the liverwort *Marchantia polymorpha*. *Plant Cell*. 2015:27(6):1650–1669. https://doi.org/10.1105/tpc.15.00065

Fox J, Weisberg S. *An R companion to applied regression*. Third edition. Thousand Oaks (CA): Sage; 2019.

Gao Y, Dai X, Aoi Y, Takebayashi Y, Yang L, Guo X, Zeng Q, Yu H, Kasahara H, Zhao Y. Two homologous INDOLE-3-ACETAMIDE (IAM) HYDROLASE genes are required for the auxin effects of IAM in *Arabidopsis*. *J Genet Genomics*. 2020:47(3):157–165. https://doi.org/10.1016/j.jgg.2020.02.009

Glawischnig E, Hansen BG, Olsen CE, Halkier BA. Camalexin is synthesized from indole-3-acetaldoxime, a key branching point between primary and secondary metabolism in *Arabidopsis*. *Proc Natl Acad Sci U S A*. 2004:101(21):8245–8250. https://doi.org/10.1073/pnas.0305876101

Grabov A, Ashley MK, Rigas S, Hatzopoulos P, Dolan L, Vicente-Agullo F. Morphometric analysis of root shape. *New Phytol*. 2005:165(2):641–652. https://doi.org/10.1111/j.1469-8137.2004.01258.x

Graves S, Piepho HP, Selzer L, Dorai-Raj S. *multcompView: visualizations of paired comparisons*. R package version 0.1-10; 2024. https://github.com/lselzer/multcompvie

Grubb CD, Zipp BJ, Ludwig-Müller J, Masuno MN, Molinski TF, Abel S. *Arabidopsis* glucosyltransferase UGT74B1 functions in glucosinolate biosynthesis and auxin homeostasis. *Plant J*. 2004:40(6):893–908. https://doi.org/10.1111/j.1365-313X.2004.02261.x

Halkier BA, Gershenzon J. Biology and biochemistry of glucosinolates. *Annu Rev Plant Biol*. 2006:57(1):303–333. https://doi.org/10.1146/annurev.arplant.57.032905.105228

Hayashi K-i, Arai K, Aoi Y, Tanaka Y, Hira H, Guo R, Hu Y, Ge C, Zhao Y, Kasahara H, et al. The main oxidative inactivation pathway of the plant hormone auxin. *Nat Commun*. 2021:12(1):6752. https://doi.org/10.1038/s41467-021-27020-1

Henbest HB, Jones ERH, Smith GF. Isolation of a new plant-growth hormone, 3-indolylacetonitrile. *J Chem Soc*. 1953:3796–3801. https://doi.org/10.1039/jr9530003796

Hobbie L, Estelle M. Genetic approaches to auxin action. *Plant Cell Environ*. 1994:17(5):525–540. https://doi.org/10.1111/j.1365-3040.1994.tb00147.x

Hull AK, Vij R, Celenza JL. *Arabidopsis* cytochrome P450s that catalyze the first step of tryptophan-dependent indole-3-acetic acid biosynthesis. *Proc Natl Acad Sci U S A*. 2000:97(5):2379–2384. https://doi.org/10.1073/pnas.040569997

Irmisch S, Zeltner P, Handrick V, Gershenzon J, Köllner TG. The maize cytochrome P450 CYP79A61 produces phenylacetaldoxime and indole-3-acetaldoxime in heterologous systems and might contribute to plant defense and auxin formation. *BMC Plant Biol*. 2015:15(1):128. https://doi.org/10.1186/s12870-015-0526-1

Kassambara A. *rstatix: pipe-friendly framework for basic statistical tests*. 2023.

Keereetaweep J, Blancaflor EB, Hornung E, Feussner I, Chapman KD. Ethanolamide oxylipins of linolenic acid can negatively regulate *Arabidopsis* seedling development. *Plant Cell*. 2013:25(10):3824–3840. https://doi.org/10.1105/tpc.113.119024

Khan BR, Faure L, Chapman KD, Blancaflor EB. A chemical genetic screen uncovers a small molecule enhancer of the N-acylethanolamine degrading enzyme, fatty acid amide hydrolase, in *Arabidopsis*. *Sci Rep*. 2017:7(1):41121. https://doi.org/10.1038/srep41121

Kim S-C, Kang L, Nagaraj S, Blancaflor EB, Mysore KS, Chapman KD. Mutations in *Arabidopsis* fatty acid amide hydrolase reveal that catalytic activity influences growth but not sensitivity to abscisic acid or pathogens. *J Biol Chem*. 2009:284(49):34065–34074. https://doi.org/10.1074/jbc.M109.059022

Kruskal WH, Wallis WA. Use of ranks in one-criterion variance analysis. *J Am Stat Assoc*. 1952:47(260):583–621. https://doi.org/10.1080/01621459.1952.10483441

Lambrix V, Reichelt M, Mitchell-Olds T, Kliebenstein DJ, Gershenzon J. The *Arabidopsis* epithiospecifier protein promotes the hydrolysis of glucosinolates to nitriles and influences *Trichoplusia ni* herbivory. *Plant Cell*. 2001:13(12):2793–2807. https://doi.org/10.1105/tpc.010261

Lavenus J, Goh T, Roberts I, Guyomarc'h S, Lucas M, De Smet I, Fukaki H, Beeckman T, Bennett M, Laplaze L. Lateral root development in *Arabidopsis*: fifty shades of auxin. *Trends Plant Sci*. 2013:18(8):450–458. https://doi.org/10.1016/j.tplants.2013.04.006

Lehmann T, Hoffmann M, Hentrich M, Pollmann S. Indole-3-acetamide-dependent auxin biosynthesis: a widely distributed way of indole-3-acetic acid production? *Eur J Cell Biol*. 2010:89(12):895–905. https://doi.org/10.1016/j.ejcb.2010.06.021

Lehmann T, Janowitz T, Sánchez-Parra B, Alonso M-MP, Trompetter I, Piotrowski M, Pollmann S. *Arabidopsis* NITRILASE 1 contributes to the regulation of root growth and development through modulation of auxin biosynthesis in seedlings. *Front Plant Sci*. 2017:8:36. https://doi.org/10.3389/fpls.2017.00036

Levene H. Robust tests for equality of variances. In: Olkin I, editor. *Contributions to probability and statistics, Olkin, I*. Palo Alto: Stanford University Press; 1960. p. 278–292.

Li J, Chen S, Zhu L, Last RL. Isolation of cDNAs encoding the tryptophan pathway enzyme indole-3-glycerol phosphate synthase from *Arabidopsis thaliana*. *Plant Physiol*. 1995:108(2):877–878. https://doi.org/10.1104/pp.108.2.877

Livak KJ, Schmittgen TD. Analysis of relative gene expression data using real-time quantitative PCR and the 2(-delta delta C(T)) method. *Methods*. 2001:25(4):402–408. https://doi.org/10.1006/meth.2001.1262

Luck K, Jirschitzka J, Irmisch S, Huber M, Gershenzon J, Köllner TG. CYP79D enzymes contribute to jasmonic acid-induced formation of aldoximes and other nitrogenous volatiles in two *Erythroxylum* species. *BMC Plant Biol*. 2016:16(1):215. https://doi.org/10.1186/s12870-016-0910-5

Marchant A, Bhalerao R, Casimiro I, Eklöf J, Casero PJ, Bennett M, Sandberg G. AUX1 promotes lateral root formation by facilitating indole-3-acetic acid distribution between sink and source tissues in the *Arabidopsis* seedling. *Plant Cell*. 2002:14(3):589–597. https://doi.org/10.1105/tpc.010354

Marchant A, Kargul J, May ST, Muller P, Delbarre A, Perrot-Rechenmann C, Bennett MJ. AUX1 regulates root gravitropism in *Arabidopsis* by facilitating auxin uptake within root apical tissues. *EMBO J*. 1999:18(8):2066–2073. https://doi.org/10.1093/emboj/18.8.2066

Marquès-Bueno MM, Armengot L, Noack LC, Bareille J, Rodriguez L, Platre MP, Bayle V, Liu M, Opdenacker D, Vanneste S, et al. Auxin-regulated reversible inhibition of TMK1 signaling by MAKR2 modulates the dynamics of root gravitropism. *Curr Biol*. 2021:31(1):228–237.e10. https://doi.org/10.1016/j.cub.2020.10.011

McCullagh P, Nelder JA. *Generalized linear models*. 2nd ed. London: CRC Press; 1989.

Merchante C, Stepanova AN. The triple response assay and its use to characterize ethylene mutants in *Arabidopsis*. *Methods Mol Biol*. 2017:1573:163–209. https://doi.org/10.1007/978-1-4939-6854-1_13

Mikkelsen MD, Hansen CH, Wittstock U, Halkier BA. Cytochrome P450 CYP79B2 from *Arabidopsis* catalyzes the conversion of tryptophan to indole-3-acetaldoxime, a precursor of indole glucosinolates and indole-3-acetic acid. *J Biol Chem*. 2000:275(43):33712–33717. https://doi.org/10.1074/jbc.M001667200

Mucha S, Heinzlmeir S, Kriechbaumer V, Strickland B, Kirchhelle C, Choudhary M, Kowalski N, Eichmann R, Hückelhoven R, Grill E, et al. The formation of a camalexin biosynthetic metabolon. *Plant Cell*. 2019:31(11):2697–2710. https://doi.org/10.1105/tpc.19.00403

Mulelu AE, Kirykowicz AM, Woodward JD. Cryo-EM and directed evolution reveal how *Arabidopsis* nitrilase specificity is influenced by its quaternary structure. *Commun Biol*. 2019:2(1):1–11. https://doi.org/10.1038/s42003-019-0505-4

Müller TM, Böttcher C, Morbitzer R, Götz CC, Lehmann J, Lahaye T, Glawischnig E. TRANSCRIPTION ACTIVATOR-LIKE EFFECTOR NUCLEASE-mediated generation and metabolic analysis of camalexin-deficient *cyp71a12 cyp71a13* double knockout lines. *Plant Physiol*. 2015:168(3):849–858. https://doi.org/10.1104/pp.15.00481

Nafisi M, Goregaoker S, Botanga CJ, Glawischnig E, Olsen CE, Halkier BA, Glazebrook J. *Arabidopsis* cytochrome P450 monooxygenase 71A13 catalyzes the conversion of indole-3-acetaldoxime in camalexin synthesis. *Plant Cell*. 2007:19(6):2039–2052. https://doi.org/10.1105/tpc.107.051383

Nonhebel HM. Tryptophan-independent indole-3-acetic acid synthesis: critical evaluation of the evidence. *Plant Physiol*. 2015:169(2):1001–1005. https://doi.org/10.1104/pp.15.01091

Normanly J, Cohen JD, Fink GR. *Arabidopsis thaliana* auxotrophs reveal a tryptophan-independent biosynthetic pathway for indole-3-acetic acid. *Proc Natl Acad Sci U S A*. 1993:90(21):10355–-10359. https://doi.org/10.1073/pnas.90.21.10355

Normanly J, Grisafi P, Fink GR, Bartel B. *Arabidopsis* mutants resistant to the auxin effects of indole-3-acetonitrile are defective in the nitrilase encoded by the NIT1 gene. *Plant Cell*. 1997:9(10):1781–1790. https://doi.org/10.1105/tpc.9.10.1781

Novák O, Hényková E, Sairanen I, Kowalczyk M, Pospíšil T, Ljung K. Tissue-specific profiling of the *Arabidopsis thaliana* auxin metabolome. *Plant J*. 2012:72(3):523–536. https://doi.org/10.1111/j.1365-313X.2012.05085.x

Ostin A, Ilic N, Cohen JD. An in vitro system from maize seedlings for tryptophan-independent indole-3-acetic acid biosynthesis. *Plant Physiol*. 1999:119(1):173–178. https://doi.org/10.1104/pp.119.1.173

Ouyang J, Shao X, Li J. Indole-3-glycerol phosphate, a branchpoint of indole-3-acetic acid biosynthesis from the tryptophan biosynthetic pathway in *Arabidopsis thaliana*. *Plant J*. 2000:24(3):327–334. https://doi.org/10.1046/j.1365-313x.2000.00883.x

Park WJ, Kriechbaumer V, Möller A, Piotrowski M, Meeley RB, Gierl A, Glawischnig E. The nitrilase ZmNIT2 converts indole-3-acetonitrile to indole-3-acetic acid. *Plant Physiol*. 2003:133(2):794–802. https://doi.org/10.1104/pp.103.026609

Pěnčík A, Simonovik B, Petersson SV, Henyková E, Simon S, Greenham K, Zhang Y, Kowalczyk M, Estelle M, Zažímalová E, et al. Regulation of auxin homeostasis and gradients in *Arabidopsis* roots through the formation of the indole-3-acetic acid catabolite 2-oxindole-3-acetic acid. *Plant Cell*. 2013:25(10):3858–3870. https://doi.org/10.1105/tpc.113.114421

Péret B, Swarup K, Ferguson A, Seth M, Yang Y, Dhondt S, James N, Casimiro I, Perry P, Syed A, et al. *AUX/LAX* genes encode a family of auxin influx transporters that perform distinct functions during *Arabidopsis* development. *Plant Cell*. 2012:24(7):2874–2885. https://doi.org/10.1105/tpc.112.097766

Perez VC, Dai R, Bai B, Tomiczek B, Askey BC, Zhang Y, Rubin GM, Ding Y, Grenning A, Block AK, et al. Aldoximes are precursors of auxins in *Arabidopsis* and maize. *New Phytol*. 2021:231(4):1449–1461. https://doi.org/10.1111/nph.17447

Perez VC, Dai R, Tomiczek B, Mendoza J, Wolf ESA, Grenning A, Vermerris W, Block AK, Kim J. Metabolic link between auxin production and specialized metabolites in *Sorghum bicolor*. *J Exp Bot*. 2023:74(1):364–376. https://doi.org/10.1093/jxb/erac421

Pérez-Alonso M-M, Ortiz-García P, Moya-Cuevas J, Lehmann T, Sánchez-Parra B, Björk RG, Karim S, Amirjani MR, Aronsson H, Wilkinson MD, et al. Endogenous indole-3-acetamide levels contribute to the crosstalk between auxin and abscisic acid, and trigger plant stress responses in *Arabidopsis*. *J Exp Bot*. 2021:72(2):459–475. https://doi.org/10.1093/jxb/eraa485

Petricka JJ, Winter CM, Benfey PN. Control of *Arabidopsis* root development. *Annu Rev Plant Biol*. 2012:63(1):563–590. https://doi.org/10.1146/annurev-arplant-042811-105501

Pickett FB, Wilson AK, Estelle M. The *aux1* mutation of *Arabidopsis* confers both auxin and ethylene resistance. *Plant Physiol*. 1990:94(3):1462–1466. https://doi.org/10.1104/pp.94.3.1462

Pollmann S, Müller A, Piotrowski M, Weiler EW. Occurrence and formation of indole-3-acetamide in *Arabidopsis thaliana*. *Planta*. 2002:216(1):155–161. https://doi.org/10.1007/s00425-002-0868-4

Pollmann S, Neu D, Lehmann T, Berkowitz O, Schäfer T, Weiler EW. Subcellular localization and tissue specific expression of amidase

1 from *Arabidopsis thaliana*. *Planta*. 2006:224(6):1241–1253. https://doi.org/10.1007/s00425-006-0304-2

Pollmann S, Neu D, Weiler EW. Molecular cloning and characterization of an amidase from *Arabidopsis thaliana* capable of converting indole-3-acetamide into the plant growth hormone, indole-3-acetic acid. *Phytochemistry*. 2003:62(3):293–300. https://doi.org/10.1016/S0031-9422(02)00563-0

Rahman A, Ahamed A, Amakawa T, Goto N, Tsurumi S. Chromosaponin I specifically interacts with AUX1 protein in regulating the gravitropic response of *Arabidopsis* roots. *Plant Physiol*. 2001:125(2):990–1000. https://doi.org/10.1104/pp.125.2.990

Rahman A, Takahashi M, Shibasaki K, Wu S, Inaba T, Tsurumi S, Baskin TI. Gravitropism of *Arabidopsis thaliana* roots requires the polarization of PIN2 toward the root tip in meristematic cortical cells. *Plant Cell*. 2010:22(6):1762–1776. https://doi.org/10.1105/tpc.110.075317

Rajagopal R, Larsen P. Metabolism of indole-3-acetaldoxime in plants. *Planta*. 1972:103(1):45–54. https://doi.org/10.1007/BF00394605

Robbins NE, Dinneny JR. Growth is required for perception of water availability to pattern root branches in plants. *Proc Natl Acad Sci U S A*. 2018:115(4):E822–E831. https://doi.org/10.1073/pnas.1710709115

Roman A, Montenegro J, Fraile L, Urra M, Buezo J, Cornejo A, Moran JF, Gogorcena Y. Indole-3-acetaldoxime delays root iron-deficiency responses and modify auxin homeostasis in *Medicago truncatula*. *Plant Sci*. 2023:332:111718. https://doi.org/10.1016/j.plantsci.2023.111718

Ruegger M, Dewey E, Gray WM, Hobbie L, Turner J, Estelle M. The TIR1 protein of *Arabidopsis* functions in auxin response and is related to human SKP2 and yeast Grr1p. *Genes Dev*. 1998:12(2):198–207. https://doi.org/10.1101/gad.12.2.198

Seo M, Akaba S, Oritani T, Delarue M, Bellini C, Caboche M, Koshiba T. Higher activity of an aldehyde oxidase in the auxin-overproducing *superroot1* mutant of *Arabidopsis thaliana*. *Plant Physiol*. 1998:116(2):687–693. https://doi.org/10.1104/pp.116.2.687

Shapiro SS, Wilk MB. An analysis of variance test for normality (complete samples). *Biometrika*. 1965:52(3–4):591–611. https://doi.org/10.1093/biomet/52.3-4.591

Shrestha R, Dixon RA, Chapman KD. Molecular identification of a functional homologue of the mammalian fatty acid amide hydrolase in *Arabidopsis thaliana*. *J Biol Chem*. 2003:278(37):34990–34997. https://doi.org/10.1074/jbc.M305613200

Shrestha R, Kim S, Dyer JM, Dixon RA, Chapman KD. Plant fatty acid (ethanol) amide hydrolases. *Biochim Biophys Acta*. 2006:1761(3):324–334. https://doi.org/10.1016/j.bbalip.2006.03.004

Spaepen S, Vanderleyden J, Remans R. Indole-3-acetic acid in microbial and microorganism-plant signaling. *FEMS Microbiol Rev*. 2007:31(4):425–448. https://doi.org/10.1111/j.1574-6976.2007.00072.x

Stepanova AN, Hoyt JM, Hamilton AA, Alonso JM. A link between ethylene and auxin uncovered by the characterization of two root-specific ethylene-insensitive mutants in *Arabidopsis*. *Plant Cell*. 2005:17(8):2230–2242. https://doi.org/10.1105/tpc.105.033365

Stepanova AN, Robertson-Hoyt J, Yun J, Benavente LM, Xie D-Y, Doležal K, Schlereth A, Jürgens G, Alonso JM. TAA1-mediated auxin biosynthesis is essential for hormone crosstalk and plant development. *Cell*. 2008:133(1):177–191. https://doi.org/10.1016/j.cell.2008.01.047

Stepanova AN, Yun J, Likhacheva AV, Alonso JM. Multilevel interactions between ethylene and auxin in *Arabidopsis* roots. *Plant Cell*. 2007:19(7):2169–2185. https://doi.org/10.1105/tpc.107.052068

Stepanova AN, Yun J, Robles LM, Novak O, He W, Guo H, Ljung K, Alonso JM. The *Arabidopsis* YUCCA1 flavin monooxygenase functions in the indole-3-pyruvic acid branch of auxin biosynthesis. *Plant Cell*. 2011:23(11):3961–3973. https://doi.org/10.1105/tpc.111.088047

Sugawara S, Hishiyama S, Jikumaru Y, Hanada A, Nishimura T, Koshiba T, Zhao Y, Kamiya Y, Kasahara H. Biochemical analyses of indole-3-acetaldoxime-dependent auxin biosynthesis in *Arabidopsis*. *Proc Natl Acad Sci U S A*. 2009:106(13):5430–5435. https://doi.org/10.1073/pnas.0811226106

Suzuki H, Yokokura J, Ito T, Arai R, Yokoyama C, Toshima H, Nagata S, Asami T, Suzuki Y. Biosynthetic pathway of the phytohormone auxin in insects and screening of its inhibitors. *Insect Biochem Mol Biol*. 2014:53:66–72. https://doi.org/10.1016/j.ibmb.2014.07.008

Tao Y, Ferrer J-L, Ljung K, Pojer F, Hong F, Long JA, Li L, Moreno JE, Bowman ME, Ivans LJ, et al. Rapid synthesis of auxin via a new tryptophan-dependent pathway is required for shade avoidance in plants. *Cell*. 2008:133(1):164–176. https://doi.org/10.1016/j.cell.2008.01.049

Thimann KV, Mahadevan S. Nitrilase: I. Occurrence, preparation, and general properties of the enzyme. *Arch Biochem Biophys*. 1964:105(1):133–141. https://doi.org/10.1016/0003-9861(64)90244-9

Tsugafune S, Mashiguchi K, Fukui K, Takebayashi Y, Nishimura T, Sakai T, Shimada Y, Kasahara H, Koshiba T, Hayashi K-i. Yucasin DF, a potent and persistent inhibitor of auxin biosynthesis in plants. *Sci Rep*. 2017:7(1):13992. https://doi.org/10.1038/s41598-017-14332-w

Vorwerk S, Biernacki S, Hillebrand H, Janzik I, Müller A, Weiler EW, Piotrowski M. Enzymatic characterization of the recombinant *Arabidopsis thaliana* nitrilase subfamily encoded by the NIT2/NIT1/NIT3-gene cluster. *Planta*. 2001:212(4):508–516. https://doi.org/10.1007/s004250000420

Wang B, Chu J, Yu T, Xu Q, Sun X, Yuan J, Xiong G, Wang G, Wang Y, Li J. Tryptophan-independent auxin biosynthesis contributes to early embryogenesis in *Arabidopsis*. *Proc Natl Acad Sci U S A*. 2015:112(15):4821–4826. https://doi.org/10.1073/pnas.1503998112

Wright AD, Sampson MB, Neuffer MG, Michalczuk L, Slovin JP, Cohen JD. Indole-3-acetic acid biosynthesis in the mutant maize *orange pericarp*, a tryptophan auxotroph. *Science*. 1991:254(5034):998–1000. https://doi.org/10.1126/science.254.5034.998

Yamada M, Greenham K, Prigge MJ, Jensen PJ, Estelle M. The *TRANSPORT INHIBITOR RESPONSE2* gene is required for auxin synthesis and diverse aspects of plant development. *Plant Physiol*. 2009:151(1):168–179. https://doi.org/10.1104/pp.109.138859

Yokoyama C, Takei M, Kouzuma Y, Nagata S, Suzuki Y. Novel tryptophan metabolic pathways in auxin biosynthesis in silkworm. *J Insect Physiol*. 2017:101:91–96. https://doi.org/10.1016/j.jinsphys.2017.07.006

Zhang Y, Berman A, Shani E. Plant hormone transport and localization: signaling molecules on the move. *Annu Rev Plant Biol*. 2023:74(1):453–479. https://doi.org/10.1146/annurev-arplant-070722-015329

Zhao Y. Auxin biosynthesis and its role in plant development. *Annu Rev Plant Biol*. 2010:61(1):49–64. https://doi.org/10.1146/annurev-arplant-042809-112308

Zhao Y. Essential roles of local auxin biosynthesis in plant development and in adaptation to environmental changes. *Annu Rev Plant Biol*. 2018:69(1):417–435. https://doi.org/10.1146/annurev-arplant-042817-040226

Zhao Y, Christensen SK, Fankhauser C, Cashman JR, Cohen JD, Weigel D, Chory J. A role for flavin monooxygenase-like enzymes in auxin biosynthesis. *Science*. 2001:291(5502):306–309. https://doi.org/10.1126/science.291.5502.306

Zhao Y, Hull AK, Gupta NR, Goss KA, Alonso J, Ecker JR, Normanly J, Chory J, Celenza JL. Trp-dependent auxin biosynthesis in *Arabidopsis*: involvement of cytochrome P450s CYP79B2 and CYP79B3. *Genes Dev*. 2002:16(23):3100–3112. https://doi.org/10.1101/gad.1035402

Zhou Z-Y, Zhang C-G, Wu L, Zhang C-G, Chai J, Wang M, Jha A, Jia P-F, Cui S-J, Yang M, et al. Functional characterization of the *CKRC1/TAA1* gene and dissection of hormonal actions in the *Arabidopsis* root. *Plant J*. 2011:66(3):516–527. https://doi.org/10.1111/j.1365-313X.2011.04509.x

Zhu T, Herrfurth C, Xin M, Savchenko T, Feussner I, Goossens A, De Smet I. Warm temperature triggers JOX and ST2A-mediated jasmonate catabolism to promote plant growth. *Nat Commun*. 2021:12(1):4804. https://doi.org/10.1038/s41467-021-24883-2